NASA TECHNICAL NOTE

NASA TN D-5699

NASA TN D-5699

AN ANALYTICAL METHOD FOR DETERMINING THE MELT-LAYER THICKNESS AND REGRESSION RATES FOR A HYBRID OR TRIBRID ROCKET MOTOR

by Walter Brooks Drew

Langley Research Center
Hampton, Va. 23365

NATIONAL AERONAUTICS AND SPACE ADMINISTRATION • WASHINGTON, D. C. • MAY 1970

1. Report No. NASA TN D-5699	2. Government Accession No.	3. Recipient's Catalog No.
4. Title and Subtitle AN ANALYTICAL METHOD FOR DETERMINING THE MELT-LAYER THICKNESS AND REGRESSION RATES FOR A HYBRID OR TRIBRID ROCKET MOTOR		5. Report Date May 1970 6. Performing Organization Code
7. Author(s) Walter Brooks Drew		8. Performing Organization Report No. L-6778 10. Work Unit No. 128-32-60-01-23
9. Performing Organization Name and Address NASA Langley Research Center Hampton, Va. 23365		11. Contract or Grant No. 13. Type of Report and Period Covered Technical Note
12. Sponsoring Agency Name and Address National Aeronautics and Space Administration Washington, D.C. 20546		14. Sponsoring Agency Code

15. Supplementary Notes

The material presented herein was included in a thesis submitted in partial fulfillment of the requirements for the degree of Master of Mechanical Engineering, University of South Carolina, Columbia, South Carolina, 1968.

16. Abstract

The investigation was originally undertaken to demonstrate the effect that an obviously important parameter, fuel thermal conductivity, has on melt-layer buildup and regression rate. Also, an interesting result of this analysis was the delineation of the effect that heat input to the fuel surface has on melt-layer buildup.

Analytical results based on laboratory-size motors indicate that the slab-burner and cylindrical-grain configurations will produce melt-layer thicknesses greater than the experimentally determined critical value for stripping of 0.125 inch (0.33 cm) and will permit the liquid fuel to be stripped away from the fuel surface by the viscous forces in the gaseous boundary layer. This condition will produce low combustion efficiencies in the tribrid rocket system.

Calculations also show that the thickness of the melt layer is a strong function of the convective and radiative heat input to the fuel surface and can be minimized by manipulating surface heat input through flow rates and grain geometry.

17. Key Words Suggested by Author(s)	18. Distribution Statement
Hybrid and tribrid rocket motors Regression rates Melt layer	Unclassified – Unlimited

19. Security Classif. (of this report)	20. Security Classif. (of this page)	21. No. of Pages	22. Price*
Unclassified	Unclassified	64	$3.00

*For sale by the Clearinghouse for Federal Scientific and Technical Information
Springfield, Virginia 22151

AN ANALYTICAL METHOD FOR DETERMINING THE MELT-LAYER THICKNESS AND REGRESSION RATES FOR A HYBRID OR TRIBRID ROCKET MOTOR*

By Walter Brooks Drew
Langley Research Center

SUMMARY

An analytical investigation was performed that produced a method whereby the regression rates and melt-layer thickness of a tribrid solid fuel could be determined. Slab-burner tests of the fuels in question substantiate the analytical method. Regression-rate studies of hybrid fuels in the past have not been concerned with the heat transferred into the grain because previous solid fuels have had low thermal conductivity and did not allow appreciable heat penetration into the grain. With the appearance of hybrid and tribrid fuels that contain a large amount of high conductivity metal, a need arose for a method of predicting regression rates that took into account a new problem that presented itself, melt-layer buildup. In order to predict melt-layer buildup, the true nature of heat transfer, liberation, and absorption in the fuel grain must be considered. The method presented has accomplished this objective.

The investigation was originally undertaken to demonstrate the effect that an obviously important parameter, fuel thermal conductivity, has on melt-layer buildup and regression rate. Also, an interesting result of this analysis was the delineation of the effect that heat input to the fuel surface has on melt-layer buildup.

Analytical results based on laboratory-size motors indicate that the slab-burner and cylindrical-grain configurations will produce melt-layer thicknesses greater than the experimentally determined critical value for stripping of 0.125 inch (0.32 cm) and will permit the liquid fuel to be stripped away from the fuel surface by the viscous forces in the gaseous boundary layer. This condition will produce low combustion efficiencies in the tribrid rocket system.

Calculations also show that the thickness of the melt layer is a strong function of the convective and radiative heat input to the fuel surface and can be minimized by manipulating surface heat input through flow rates and grain geometry.

---

*The material presented herein was included in a thesis submitted in partial fulfillment of the requirements for the degree of Master of Mechanical Engineering, University of South Carolina, Columbia, South Carolina, 1968.

INTRODUCTION

The hybrid rocket propulsion system utilizes a solid-fuel grain with a liquid oxidizer sprayed across the grain surface. Research has developed the technology necessary for the production of a flight hybrid system, and the hybrid concept has been satisfactorily demonstrated.

The "tribrid" rocket propulsion system is a natural extension of the hybrid technology. The difference between the two concepts lies in mixing a third nonworking gas component into the hot hybrid combustion products. The best fluid to be added in this manner is hydrogen, because of its low molecular weight. The consequences of adding hydrogen to the hybrid system are advantageous in two ways. First, the temperature of the gases entering the rocket nozzle is reduced from above 8000° F (4426° C) to below 3000° F (1649° C) for this study. The advantages of lower nozzle temperature appear in simpler fabrication techniques, lower weight, and better reliability. Second, the specific impulse is increased since it is proportional to the square root of the stagnation temperature divided by the molecular weight of the exhaust gases, and at some percentage H_2, these parameters will produce a maximum specific impulse. Figure 1 shows a schematic of a tribrid rocket motor.

The particular tribrid system under study in this investigation is composed of liquid fluorine as the oxidizer, lithium as the fuel, and hydrogen as the nonworking component. The theoretical specific impulse I_S for this system is 511 seconds, as compared with 478 seconds for the liquid hydrogen, fluorine rocket which represents the highest yield liquid rocket motor, and 440 seconds for high-performance hybrid motors. This increased specific impulse is expected to more than offset the additional hydrogen tankage requirements.

Preliminary slab burner tests of the tribrid system performed by R. J. Muzzy of United Technology Center indicate that a major problem exists when employing a lithium fuel as the solid grain. This problem occurs when the lithium fuel melts faster than it can be vaporized and burned. After a 0.33-cm-thick layer of melted lithium forms on the surface, it will be stripped away by the viscous forces of the boundary-layer gases. When this condition occurs, the unburned lithium is exhausted and high inefficiencies occur in the system. This liquid layer is produced on the lithium fuel because the fuel has a high thermal conductivity at a high temperature (≈2400° F (1315° C)). Also, lithium has a large heat of vaporization as compared with the heat of fusion (186 Btu/lb (103.3 cal/g)) at a temperature of 356° F (166° C). These physical characteristics allow energy to be transferred into the grain at a rate larger than the rate at which the surface is burned away.

A proposed solution to this problem is to decrease the thermal conductivity of the fuel grain by mixing the lithium with a low thermal conductivity hydrocarbon solid fuel and adding an appropriate amount of oxygen to the fluorine in order to burn this fuel. This approach to the problem appears to be feasible, but it has an inherent drawback because of the fact that the more hydrocarbon binder that is added, the lower the specific impulse will be. Also, after a certain amount of binder has been added, self-sustaining solid reactions will occur. Analytical studies have shown that a 90-percent lithium, 10-percent binder is theoretically capable of 502 seconds; an 80-percent lithium, 20-percent binder will produce 491 seconds specific impulse; and if the lithium content is reduced to 70 percent, the specific impulse will drop to 480 seconds.* From these numbers the importance of determining the minimum amount of binder required to prevent melt-layer buildup is appreciated.

Herein lies an important objective of this study – to determine analytically the minimum amount of binder necessary in order to prevent the formation of a melt layer on the tribrid fuel grain surface that could be stripped away by the viscous shear forces of the reacting boundary layer.

It is obvious that the melt-layer thickness is directly related to the difference between surface and melt-layer regression rates. Regression-rate studies of hybrid fuels in the past have not been properly concerned with the internal heat transferred into the grain because previous hybrid fuels have had low thermal conductivity and did not allow an appreciable amount of internal heat transfer by conduction. In order to predict melt-layer buildup on a lithium fuel, all aspects of heat transfer in the fuel grain must be considered.

An analytical solution to this problem, which is dependent upon experimental values for surface temperature, is presented. The solution was accomplished by using established methods to determine the heat transferred from the turbulent reacting boundary layer by convection and radiation to the fuel surface. The analysis considers the heat of vaporization of the fuel at the surface, the conduction through a melt layer to the solid-melt interface (the heat of fusion being taken into account at this point) and finally, conduction into the solid grain.

This investigation was originally undertaken to demonstrate the effect that an obviously important parameter, fuel thermal conductivity, has on melt-layer buildup and regression rates. The results of the analysis also made clear the influence of the heat input to the surface from boundary-layer convection and radiation. Details of the method are presented herein.

---

*This information was obtained informally from unpublished data supplied by the Propulsion Branch of the Langley Research Center.

SYMBOLS

A area, in^2 (cm^2)

$A_i = \Delta t\, K\left(-\frac{1}{\Delta r^2} + \frac{1}{2r_i\, \Delta r}\right)$, dimensionless

B mass transfer number, dimensionless, $\frac{u_e}{u_b}\frac{\Delta h}{h_v}$

B_i constant, $1 + \frac{2\,\Delta t\, K}{\Delta r^2}$, dimensionless

$B' = B \times N_{Pr}^{-0.67}$, dimensionless

C constant

C_f skin-friction coefficient, dimensionless

D known constants of simultaneous equations

H sensible enthalpy, Btu/lb (cal/mole)

ΔH sensible enthalpy difference between flame and wall, Btu/lb (cal/mole)

K mass fraction of nonvaporizing matter $\frac{k}{\rho c_p}$, in^2/sec (cm^2/sec)

$K_1 = \frac{2\,\Delta t\, K}{\Delta r\, k}$, $sec\text{-}^oF\text{-}in^2/Btu$ $(sec\text{-}^oC\text{-}cm^2/cal)$

$K_2 = 1 + \frac{2\,\Delta t\, K}{\Delta r^2}$, dimensionless

$K_3 = \frac{2\,\Delta t\, k}{\Delta r^2}$, dimensionless

$K_{O,e}$ oxidizer concentration in free stream

L_v heat of vaporization of vaporizing component, Btu/lb (cal/mole)

N radiation parameter, dimensionless; also as integer

N_{Pr} Prandtl number, dimensionless, $\frac{c_p \mu}{k}$

N_{Re}	Reynolds number, dimensionless, $\frac{\rho u d}{\mu}$
N_{St}	Stanton number, dimensionless, $\frac{h}{c_p \rho_b u_b}$
O/F	oxidizer to fuel ratio
$\dot{Q}$	heat transfer, Btu/in^2-sec (cal/cm^2-sec)
R	radiation, Btu/in^2-sec (cal/cm^2-sec)
R_o, R_{bs}	initial and back side radii, respectively
T	temperature, ^oF (^oC)
Z	radiative path length, in. (cm)
c_p	specific heat, Btu/lb-^oF (cal/deg mole)
d_m	melt-layer thickness, in. (cm)
h	convective heat-transfer coefficient, Btu/in^2-^oF-sec (cal/cm^2-^oC-sec)
h_v	heat of gasification of vaporizing component, Btu/lb (cal/mole)
k	coefficient of thermal conductivity, Btu/in-sec-^oF (cal/cm-^oC-sec)
$\dot{m}$	mass-transfer rate, lb/sec-in^2 (g/sec-cm^2)
r,θ,z	cylindrical coordinates
$\dot{r}$	regression rate, in./sec (cm/sec)
t	time, sec
u	velocity, in./sec (cm/sec) (in x direction)
x,y	rectangular coordinates, in. (cm)
α	empirical radiation constant, dimensionless

ϵ	emissivity, $Btu/in^2\text{-}sec$ $(cal/cm^2\text{-}sec)$
μ	viscosity, $lb\text{-}sec/in^2$ $(g\text{-}sec/cm^2)$
ρ	density, lb/in^3 (g/cm^3)
ρ_b	density of nonvaporizing component, lb/in^3 (g/cm^3)
σ	Stefan-Boltzmann constant, 0.1713×10^{-8} $Btu/ft^2\text{-}hr\text{-}^oR^4$ $(cal/cm^2\text{-}sec\text{-}^oC^4)$
τ	skin friction, lb/in^2 (g/cm^2)

Subscripts:

b	flame zone
bs	back surface
c	convection
cs	conducted from surface
e	edge of boundary layer
f	fuel
in	radiation and convection to the surface
l	liquid
m	melt
o	initial value
r	radiation
Δr	space increment

s	solid
v	vaporization
w	wall
x	x-direction
t	time
Δt	time increment

ANALYSIS

The basic theory involved in this study can be divided into two parts: First, the heat convected and radiated to the fuel surface must be established by considering a turbulent reacting gaseous boundary layer above the solid fuel. Second, the utilization of this energy in the fuel grain is treated in detail, generally through the use of numerical methods. Means for determining the physical parameters associated with the gaseous boundary layer and solid fuel are given. A computer program was produced that will make the analysis more readily usable.

Method for Calculating Heat Input to Fuel Surface

Marxman and Wooldridge have shown transition between laminar and turbulent flow occurring at $N_{Re} = 10^4$ (refs. 1 and 2) for the typical hybrid application. This transition produces turbulent flow under typical conditions. They assumed steady-state conditions where all the heat transferred to the surface is balanced by the mass-flow rate of fuel coming from the surface multiplied by the total heat of gasification of the fuel; that is,

$$\dot{Q}_w = \dot{m}_f h_v = \rho_f \dot{r} h_v \tag{1}$$

where

$\dot{m}_f$	mass rate of fuel leaving surface
h_v	an effective heat of gasification
ρ_f	density of fuel
$\dot{r}$	regression rate of fuel surface, $\frac{\partial r}{\partial t}$

Although h_v is composed of the heat of vaporization and the heat required to bring the internal energy of the grain up to the vaporization temperature, the true nature of heat conduction into the grain has been avoided. (See refs. 1 and 2.) In past studies, this assumption has been justified by the fact that solid-fuel rocket grains are thermal insulators.

The heat into the wall is divided into two parts: that due to convection and that due to radiation. Convective heat transfer in a turbulent reacting boundary layer is discussed first. In order to clarify the terminology initially, let us consider figure 2.

Convective heat transferred into the grain surface can be expressed as

$$\dot{Q}_{cw} = -\frac{h}{c_p}\left(\frac{\partial H}{\partial y}\right)_w \tag{2}$$

In equation (2), it appears that the dimension y has been normalized. At this point the Stanton number N_{St} is defined as

$$N_{St} = \frac{h}{c_p \rho_b u_b}$$

and equation (2) becomes

$$\dot{Q}_{cw} = N_{St} \rho_b u_b \Delta H \tag{3}$$

where N_{St} is based on a ΔH that is equal to the sensible enthalpy difference between the flame and the wall $\left(\Delta H = (c_p T)_b - (c_p T)_w, \text{ Btu/lb, where } c_p \text{ is the specific heat of the gases at the point in question}\right)$.

Combining equations (1) and (3) yields an expression for the regression rate

$$\dot{r} = N_{St} \frac{\rho_b}{\rho_f} u_b \frac{\Delta H}{h_v} \tag{4}$$

Equation (4) can be made usable by expressing N_{St} in terms of the skin-friction coefficient C_f since experimental data and empirical expressions are available for C_f. To do so, the Reynolds analogy between heat transfer and the local skin friction is used. For a nonunity Prandtl number, this relationship takes the modified form

$$\frac{\dot{Q}_w}{\Delta H} = \frac{\tau_w}{u_b} N_{Pr}^{-0.67} \tag{5}$$

From the definition of C_f,

$$C_f = \frac{2\tau_w}{\rho_e u_e^2} \tag{6}$$

Substituting equation (5) into equation (6) yields

$$\dot{Q}_w = \frac{C_f}{2} \frac{\rho_e u_e^2}{u_b} N_{Pr}^{-0.67} \Delta H \tag{7}$$

and equation (7) into equation (3) yields

$$N_{St} \rho_b u_b \Delta H = \frac{C_f}{2} \frac{\rho_e u_e^2}{u_b} N_{Pr}^{-0.67} \Delta H \tag{8}$$

Now an expression for N_{St} in terms of $C_f/2$ can be formed,

$$N_{St} = \frac{C_f}{2} \frac{\rho_e u_e^2}{\rho_b u_b^2} N_{Pr}^{-0.67} \tag{9}$$

Substituting this expression for N_{St} into the regression rate (eq. (4)) yields

$$\dot{r} = \frac{C_f}{2} \frac{\rho_e u_e^2}{\rho_b u_b^2} N_{Pr}^{-0.67} \frac{\rho_b}{\rho_f} u_b \frac{\Delta H}{h_v} \tag{10}$$

At this point it is convenient to define a mass transfer number B which has been modified to account for the effects of a reacting boundary layer (ref. 3).

$$B = \frac{u_e}{u_b} \frac{\Delta H}{h_v}$$

and the regression rate equation (eq. (10)) becomes

$$\dot{r} = \frac{\rho_e u_e}{\rho_f} \frac{C_f}{2} N_{Pr}^{-0.67} B \tag{11}$$

Because the definition of B takes into account physical properties of both the solid and gas phase, it is regarded as a thermochemical constant that characterizes the particular propellant. And further, B' is defined as $B \times N_{Pr}^{-0.67}$ and this parameter is the similarity parameter of a boundary layer with mass injection. (See ref. 2.)

Because the Prandtl number of a gas is near unity for a turbulent boundary layer, B serves a dual role as a thermochemical and boundary-layer flow parameter. In order to put equation (11) into a useful form, the friction coefficient C_f must be determined for a turbulent boundary layer with mass addition and combustion.

The turbulent skin-friction coefficient for a Newtonian fluid is given by Schlichting (ref. 4) as

$$\frac{C_{f,o}}{2} = 0.03 N_{Re,x}^{-0.2} \tag{12}$$

Marxman and Wooldridge (ref. 2) have shown that the effects of mass injection upon the friction coefficient can be expressed by

$$\frac{C_f}{C_{f,o}} = \left[\frac{\log_e(1 + B')}{B'}\right]^{0.8} \left[\frac{1 + \frac{13B'}{10} + \frac{4B'^2}{11}}{(1 + B')\left(1 + \frac{B'}{2}\right)^2}\right]^{0.2} \tag{13}$$

and a much simpler formula can be used in the range $5 < B' < 100$ which typifies hybrid operation

$$\frac{C_f}{C_{f,o}} = 1.2 B'^{-0.77} \tag{14}$$

Combustion affects the skin-friction coefficient by creating variable properties in the boundary layer. Investigators (refs. 5, 6, 7, and 8) have shown that this effect can be accounted for by correcting ρ_e by a density ratio of the form $\left(\bar{\rho}/\rho_e\right)^{0.6}$ where $\bar{\rho}/\rho_e$ is a suitably defined reference density. For most hybrids this ratio can be taken as unity. (See ref. 8.)

By substituting equations (12) and (14) into equation (11), the final expression for the regression rate is obtained:

$$\dot{r} = \frac{0.036}{\rho_f}\left(\frac{\bar{\rho}}{\rho_e}\right)^{0.6} u_e B'^{0.23} N_{Re,x}^{-0.2} \tag{15}$$

Two basic assumptions have been made in deriving equation (15):

(1) The applicability of the Reynolds analogy

(2) That a boundary-layer treatment is valid even for the relatively high rates of surface mass flux encountered in hybrid operation.

Assumption (1) was justified by Wooldridge and Muzzy in reference 9. These investigators showed that the turbulent Prandtl number, Schmidt number, and therefore, the Lewis number were unity. This statement was verified both analytically and experimentally.

As far as assumption (2) is concerned, velocity profile measurements by Mickley and Davis (ref. 10) and Wooldridge and Muzzy (ref. 9) show excellent agreement with the semiempirical, explicit-form velocity-profile equations up to values of B' of 100. All practical hybrid or tribrid rocket motors fall within this range.

At the present time there are many controversial aspects concerning the theoretical model and the physical reality, but it is the opinion of the author that the presented approach is the best available. The radiative heat transfer to the grain surface has been described by Marxman (refs. 2 and 8) as

$$\dot{Q}_r = \sigma \epsilon_w T_r^4 \left(1 - e^{-\alpha N Z}\right) \tag{16}$$

where

σ	Stefan-Boltzmann constant
ϵ_w	emissivity of wall
T_r	effective radiation temperature
α	empirical radiation coefficient
N	radiation parameter
Z	radiative path length

The form of equation (16) has had recent modifications; however, the presented form is considered to be adequate for this particular application.

The energy reaching the fuel surface cannot be expressed by a simple addition of the heat due to convection and radiation. A complication arises because as the surface absorbs the radiative heat, this heat increases the regression rate and therefore the blocking effects tend to reduce the convective heating. The following formula has been shown (ref. 8) to express this relationship

$$\rho_f \dot{r} = \frac{\dot{Q}_{cw}}{h_v}\left(e^{-\dot{Q}_r/\dot{Q}_{cw}} + \frac{\dot{Q}_r}{\dot{Q}_{cw}}\right) \tag{17}$$

where $\dot{Q}_{cw}$ is the convective heat transfer in the absence of radiation. It might be noted that for small values of $\dot{Q}_r/\dot{Q}_{cw}$, the trade-off is nearly exact and the regression rate may be calculated with little error by using $\dot{Q}_{cw}$ alone.

Many hybrid and tribrid rocket systems contain a high percentage of metal loading in the grain. This metal can create significant radiative heat transfer if its combustion products are solid, but if the combustion products are gaseous, little radiation will be exhibited; therefore, the effects of metal particle loading have been investigated for both radiative and nonradiative systems.

Reference 3 indicates that mass addition of particles in the flow has little effect on the shear stress distribution or velocity profile shape inside the boundary layer. This statement means that the addition of particles from the surface will not affect the relationships between C_f and $C_{f,o}$. The blocking effects which reduce C_f should be dependent only on the gas phase inside the boundary layer as long as the solid particles occupy a negligible volume compared with that of the gas. This condition would have to be satisfied in any real situation. Because of this requirement, the regression-rate equation should be written in terms of the component in the grain that produces these boundary-layer gases. This phenomenon can be taken into account by defining an effective heat of gasification as (ref. 3)

$$\rho_v h_{v,eff} = \rho_v \left(h_{v,b} + \frac{K}{K - 1} C_m \Delta T \right) \tag{18}$$

where

ρ_v density of vaporizing component

C_m specific heat of nonvaporizing component

ΔT temperature difference between surface and ambient deep in grain

K mass fraction of nonvaporizing matter

$h_{v,b}$ heat of gasification of vaporizing component

Equation (18) illustrates the fact that one component is heated to the surface temperature and vaporized, whereas the other component is heated only to the surface temperature.

Generation of a Regression-Rate Temperature-Profile Matrix

The preceding section gave a method whereby the heat input to the grain surface could be calculated. Now the problem is to represent mathematically the distribution of this heat energy inside the fuel grain. The physical situation is as follows:

(1) Fuel is vaporized at the surface by absorbing that amount of heat of vaporization.

(2) Energy is transferred across the melt layer and absorbed by increasing the internal energy of the fuel in the melt layer.

(3) At the melt-solid interface the heat of fusion of the fuel is subtracted from the total heat input from the surface.

(4) Energy is transferred by conduction from the melt-solid interface into the solid grain and thus the internal energy of the solid fuel is increased.

Carslaw and Jaeger (ref. 11) have stated that apart from the few exact solutions (concerning phase change) all problems have to be attacked by numerical methods, and that numerical techniques have the advantage that the variation in the thermal properties with temperature can be taken into account. A numerical solution was utilized for this analysis and it proceeds as follows:

The partial differential equation that describes the heat flux through a cylinder with $\partial^2 T/\partial\theta^2 = 0$ is

$$\frac{\partial T}{\partial t} = K\left(\frac{\partial^2 T}{\partial r^2} + \frac{1}{r}\frac{\partial T}{\partial r} + \frac{\partial^2 T}{\partial z^2}\right) \qquad \left(K = \frac{k}{\rho c_p}\right) \tag{19}$$

Experimental results that are available for the tribrid rocket motor indicate that the temperature variation with respect to z is small, and therefore, $\partial^2 T/\partial z^2$ can be eliminated.

It was decided to use a backward difference numerical solution that is unconditionally stable (refs. 12 and 13) for the heat-transfer equation expressed in Cartesian coordinates coupled with a method that would insure convergence. From the computer runs it appears that no stability problems exist when the more complex cylindrical coordinates are used. The backward difference is similar in formulation to the explicit method except that the derivatives are calculated at the future time level. In order to do this calculation, equation (19) was put into finite-difference form and the temperature of a block at the present time t was expressed in terms of its temperature and the temperature of the surrounding blocks at the future time $t + \Delta t$.

$$\frac{\partial T}{\partial t} = \frac{T_{i,t+\Delta t} - T_{i,t}}{\Delta t} \tag{20a}$$

$$\frac{\partial^2 T}{\partial r^2} = \frac{1}{\Delta r^2}\left(T_{(i+1)t+\Delta t} - 2T_{i,t+\Delta t} + T_{(i-1)t+\Delta t}\right) \tag{20b}$$

$$\frac{\partial T}{\partial r} = \frac{1}{2\,\Delta r}\left(T_{(i+1)t+\Delta t} - T_{(i-1)t+\Delta t}\right) \tag{20c}$$

Equations (20a), (20b), and (20c) can be substituted into equation (19) to obtain

$$-\frac{T_{i,t+\Delta t} + T_{i,t}}{\Delta t} = -K\left[\frac{1}{\Delta r^2}\left(T_{(i+1)t+\Delta t} - 2T_{i,t+\Delta t} + T_{(i-1)t+\Delta t}\right)\right.$$

$$\left. + \frac{1}{r_i}\left(\frac{1}{2\,\Delta r}\right)\left(T_{(i+1)t+\Delta t} - T_{(i-1)t+\Delta t}\right)\right] \tag{20d}$$

and solving equation (20d) for $T_{i,t}$ yields

$$T_{i,t} = \left(\frac{\Delta t\,K}{2r_i\,\Delta r} - \frac{\Delta t\,K}{\Delta r^2}\right)T_{(i-1)t+\Delta t} + \left(1 + \frac{2\,\Delta t\,K}{\Delta r^2}\right)T_{i,t+\Delta t} - \left(\frac{\Delta t\,K}{\Delta r^2} + \frac{\Delta t\,K}{2r_i\,\Delta r}\right)T_{(i+1)t+\Delta t} \tag{21}$$

Now a set of N simultaneous equations with N unknowns for each time step Δt can be formed. This equation is the general equation for the nonsteady conduction into a cylindrical solid. At this point the necessary boundary conditions that represent our particular problem must be imposed.

Because the basic equation is parabolic, initial conditions, $t = 0$, and boundary conditions at $r = R_o$ and $r = R_{bs}$ (fig. 3) must be known. The present problem also consists of defining the boundary conditions at the interface between the solid and liquid or at $r = R_m$. The initial conditions ($t = 0$) will be assumed as:

> A very thin melt layer of at least four blocks. The first block will be at the surface temperature T_o; the next three blocks will decrease linearly from T_o to the melt temperature T_m. The blocks from the fourth block to the back-insulated wall R_{bs} will be at some approximate ambient temperature T_a.

The surface boundary condition is established as follows:

$$\left.\begin{aligned} \dot{Q}_{(\text{conducted into surface})} &= -k\left.\frac{\partial T}{\partial r}\right|_{r=R_o} \\ \frac{1}{k}\dot{Q}_{cs} &= -\frac{T_{i,t+\Delta t} - T_{-1,t+\Delta t}}{2\,\Delta r} \\ T_{-1,t+\Delta t} &= T_{1,t+\Delta t} + \frac{2\,\Delta r}{k}\dot{Q}_{cs} \end{aligned}\right\} \tag{22}$$

Because mass removal at the surface exists and must be taken into account, an energy balance at the surface may be written

$$\dot{Q}_{in} = -k \frac{\partial T}{\partial r} + \rho_f \frac{\partial r}{\partial t} h_v$$

$\dot{Q}_{(\text{radiation and convection to the surface})} = \dot{Q}_{(\text{conducted from surface})} + \dot{Q}_{(\text{vaporized})}$

$$\dot{Q}_{in} = \dot{Q}_{cs} + \dot{Q}_v$$

The term $\dot{Q}_{in}$ can be obtained from equation (17), and

$$\dot{Q}_v = \rho_f \dot{r} h_v$$

where

ρ_f density of fuel

$\dot{r}$ rate of surface regression with respect to time

h_v heat of gasification of fuel

Then

$$\dot{Q}_{cs} = \dot{Q}_{in} - \rho_f \dot{r} h_v \tag{23}$$

Equation (23) can be substituted into equation (22) to obtain

$$T_{-1,t+\Delta t} = T_{1,t+\Delta t} + \frac{2\,\Delta r}{k}\left(\dot{Q}_{in} - \rho_f \dot{r} h_v\right) \tag{24}$$

Equation (24) can be substituted into equation (21) and the resulting equation is the first equation in the set of simultaneous equations. The procedure is as follows:

At the surface equation (21) takes the form

$$T_{o,t} = \left(\frac{\Delta t\, K}{2r_o\, \Delta r} - \frac{\Delta t\, K}{\Delta r^2}\right) T_{-1,t+\Delta t} + \left(1 + \frac{2\,\Delta t\, K}{\Delta r^2}\right) T_{o,t+\Delta t} - \left(\frac{\Delta t\, K}{\Delta r^2} + \frac{\Delta t\, K}{2r_o\, \Delta r}\right) T_{1,t+\Delta t} \tag{25}$$

Substitute equation (24) into equation (25) and let

$$a = \frac{\Delta t K}{2 r_o \Delta r}$$

$$b = \frac{\Delta t K}{\Delta r^2}$$

$$T_{o,t} = (a - b)\left(T_{1,t+\Delta t} + \frac{2\Delta r}{k}\dot{Q}_{cs}\right) + (1 + 2b)T_{o,t+\Delta t} - (a + b)T_{1,t+\Delta t}$$

This equation reduces to

$$T_{o,t} = (1 + 2b)T_{o,t+\Delta t} - 2bT_{1,t+\Delta t} + (a - b)\frac{2\Delta r}{k}\dot{Q}_{cs} \tag{26}$$

Because of the numerical method used, Δr at the surface must be much smaller than r_o and therefore b, the term with Δr^2 in the denominator will be much greater than a. It therefore appears to be a safe assumption that the term a in equation (26) can be neglected. Equation (26) takes the form

$$T_{o,t} = \left(1 + \frac{2\Delta t K}{\Delta r^2}\right)T_{o,t+\Delta t} - \frac{2\Delta t K}{\Delta r^2}T_{1,t+\Delta t} - \frac{2\Delta t K}{\Delta r k}\left(\dot{Q}_{in} - \rho_f \dot{r} h_v\right) \tag{27}$$

From equation (27) it is seen that a new unknown $\dot{r}$ has been added to the set of simultaneous equations and now there are N equations and N + 1 unknowns. Therefore, the assumption is made that the surface temperature T_o is known, and that it is constant for every time step or $T_{o,t} = T_{o,t+\Delta t}$. Experiment and theory indicate that this assumption is reasonable. Equation (27) becomes

$$T_{o,t}\left(K_2 - 1\right) = K_1\left(\dot{Q}_{in} - \rho_f \dot{r} h_v\right) + K_3 T_{1,t+\Delta t} \tag{28}$$

where

$$K_1 = \frac{2\Delta t K}{\Delta r k}$$

$$K_2 = \left(1 + \frac{2\Delta t K}{\Delta r^2}\right)$$

$$K_3 = \frac{2\Delta t K}{\Delta r^2}$$

Equation (28) reduces to

$$\left(T_{o,t} - \frac{K_1}{K_2 - 1}\dot{Q}_{in}\right) = \left(\frac{K_3}{K_2 - 1}\right)T_{1,t+\Delta t} - \left(\frac{\rho h_v K_1}{K_2 - 1}\right)\dot{r} \tag{29}$$

where the left-hand side of equation (29) is considered to be known; the unknowns are $T_{1,t+\Delta t}$ and $\dot{r}$. Equation (29) is the first equation in the set of N equations.

The second equation in the set of N simultaneous equations is based on equation (21):

$$T_{1,t} = A_1 T_{o,t+\Delta t} + B_i T_{1,t+\Delta t} + C_1 T_{2,t+\Delta t}$$

where

$$A_1 = \Delta t\, K\left(-\frac{1}{\Delta r^2} + \frac{1}{2r_1\,\Delta r}\right)$$

$$B_i = 1 + \frac{2\,\Delta t\, K}{\Delta r^2}$$

$$C_1 = -\Delta t\, K\left(\frac{1}{2r_1\,\Delta r} + \frac{1}{\Delta r^2}\right)$$

and $T_{o,t+\Delta t}$ is considered to be known. Therefore,

$$T_{1,t} - A_1 T_{o,t+\Delta t} = B_i T_{1,t+\Delta t} + C_1 T_{2,t+\Delta t} \tag{30}$$

The third equation is

$$T_{2,t} = A_2 T_{1,t+\Delta t} + B_i T_{2,t+\Delta t} + C_2 T_{3,t+\Delta t} \tag{31}$$

where

$$A_2 = \Delta t\, K\left(\frac{1}{\Delta r^2} + \frac{1}{2r_o\,\Delta r}\right)$$

$$C_2 = -\Delta t\, K\left(\frac{1}{2r_o\,\Delta r} - \frac{1}{\Delta r^2}\right)$$

From here on the equations take on a repetitive form until the melt-solid interface is reached. This general equation, for the (i-1) block, is

$$T_{(i-1)t} = A_{(i-1)}T_{(i-2)t+\Delta t} + B_i T_{(i-1)t+\Delta t} + C_{(i-1)}T_{i,t+\Delta t} \tag{32}$$

where

$$A_{(i-1)} = \Delta t\, K\left(\frac{1}{\Delta r^2} + \frac{1}{2r_{(i-1)}\,\Delta r}\right)$$

$$C_{(i-1)} = -\Delta t\, K\left(\frac{1}{2r_{(i-1)}\,\Delta r} - \frac{1}{\Delta r^2}\right)$$

At this point the solid-liquid interface must be considered. Note the following figure:

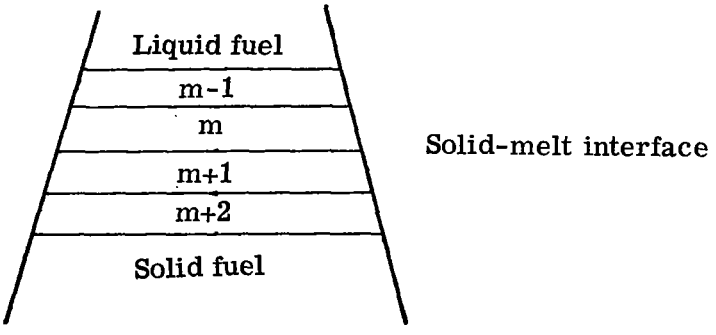

The fact that m is a moving interface with heat absorption can be taken into account by performing the following heat balance:

$$\dot{Q}_{(\text{conducted into } m)} = \dot{Q}_{(\text{heat of fusion})} + \dot{Q}_{(\text{conducted out of } m)}$$

$$k_l \left.\frac{\partial T_l}{\partial r}\right|_{r=r_m} - k_s \left.\frac{\partial T_s}{\partial r}\right|_{r=r_m} = \rho \frac{\partial r}{\partial t} h_m$$

where the subscript l represents a liquid and the subscript s represents a solid. Thus,

$$\dot{Q}_{c,in} = \dot{Q}_m + \dot{Q}_{cs} \tag{33}$$

where

$$\dot{Q}_{c,in} = \frac{kA_m}{\Delta r}\left(T_{(m-1)} - T_m\right)$$

$$\dot{Q}_m = \rho_f h_m \dot{r}_m$$

$$\dot{Q}_{cs} = \frac{kA_{(m+1)}}{\Delta r}\left(T_m - T_{(m+1)}\right)$$

Equation (33) becomes

$$\frac{kA_m}{\Delta r}\left(T_{(m-1)} - T_m\right) = \rho_f h_m \dot{r}_m + \frac{kA_{(m+1)}}{\Delta r}\left(T_m - T_{(m+1)}\right) \tag{34}$$

Because Δr is small, it can be assumed that $A_m \approx A_{(m+1)}$. At this point it is noted that the energy balances performed on the surface and at the solid-liquid interface are not in cylindrical coordinates as is the general equation (21). Therefore, the area change between the surface and the interface must be taken into account. This change is determined by setting $A_{surface} = 1$ and since θ and z are constant for all r

$$A_m = A_s \frac{r_m}{r_o} = \frac{r_m}{r_o}$$

By taking this fact into account, equation (34) is solved for T_m. Here the solution is for T_m instead of $T_{(m+1)}$; this procedure simplifies the equation

$$T_{m,t+\Delta t} = \frac{1}{2} T_{(m-1)t+\Delta t} + \left(\frac{\Delta r\, r_o \rho h_m}{2kr_m}\right)\dot{r}_m + \frac{1}{2} T_{(m+1)t+\Delta t} \tag{35}$$

Now substitute equation (35) into all equations containing T_m as follows, and thereby introduce the desired quantity $\dot{r}_m$, the regression rate of the solid-liquid interface. At this point the assumption is made that T_m is known and that it is a constant.

By following this procedure for the $(m-1)$ block,

$$T_{(m-1)t} = A_{(m-1)} T_{(m-2)t+\Delta t} + \left(B + \frac{C_{(m-1)}}{2}\right) T_{(m-1)t+\Delta t}$$

$$+ C_{(m-1)}\left(\frac{\Delta r\, r_o \rho h_m}{kr_m}\right)\dot{r}_m + \frac{C_{(m-1)}}{2} T_{(m+1)t+\Delta t} \tag{36}$$

For the mth block,

$$T_{m,t} = \left(A_m + \frac{B}{2}\right)T_{(m-1)t+\Delta t} + B\left(\frac{\Delta r\, r_o \rho h_m}{2kr_m}\right)\dot{r}_m + \left(\frac{B}{2} + C_m\right)T_{(m+1)t+\Delta t} \tag{37}$$

For the (m+1) block

$$T_{(m+1)t} = \frac{A_{(m+1)}}{2} T_{(m-1)t+\Delta t} + A_{(m+1)}\left(\frac{\Delta r\, r_o \rho h_m}{kr_m}\right)\dot{r}_m$$

$$+ \left(\frac{A_{(m+1)}}{2} + B\right)T_{(m+1)t+\Delta t} + C_{(m+1)t+\Delta t} \tag{38}$$

Equations (29), (30), (38), and (37) must be included in the melt layer, and therefore, four blocks are necessary. The rest of the equations in the interior of the solid are of the general form of equation (21).

Now consider the insulated back surface (designated by bs). Note the following sketch:

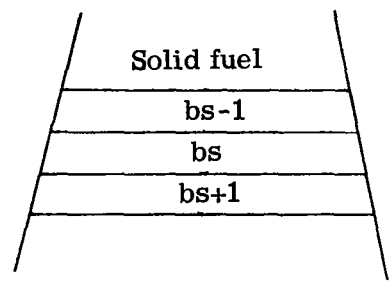

The boundary condition for an insulated back is that no heat is transferred, or

$$\dot{Q} = -k\left.\frac{\partial T}{\partial r}\right|_{r=R_{bs}}$$

$$-k\left[\frac{T_{bs+1} - T_{bs}}{\Delta r}\right] = 0$$

Therefore

$$T_{bs+1} = T_{bs}$$

To eliminate the temperature T_{bs+1} from the system of equations, let

$$T_{bs,t} = A_{bs}T_{bs-1} + \left(B + C_{bs}\right)T_{bs} \tag{39}$$

At this point the system of simultaneous equations are complete and they take the following form:

$$-\left(\frac{\rho h_v K_2}{K_2 - 1}\right)\dot{r} + \left(\frac{K_3}{K_2 - 1}\right)T_{1,t+\Delta t} = T_{o,t} - \frac{K_1}{K_2 - 1}\dot{Q}_{in}$$

$$B_i T_{1,t+\Delta t} + C_1 T_{2,t+\Delta t} = T_{1,t} - A_1 T_{o,t}$$

$$A_2 T_{1,t+\Delta t} + B_i T_{2,t+\Delta t} + C_2 T_{3,t+\Delta t} = T_{2,t}$$

$$\vdots \qquad\qquad \vdots$$

$$A_i T_{(i-1)t+\Delta t} + B_i T_{i,t+\Delta t} + C_i T_{(i+1)t+\Delta t} = T_{i,t}$$

$$A_{(m-2)} T_{(m-3)t+\Delta t} + B_i T_{(m-2)t+\Delta t} + C_{(m-2)} T_{(m-1)t+\Delta t} = T_{(m-2)t}$$

$$A_{(m-1)} T_{(m-2)t+\Delta t} + \left(B_i + \frac{C_{(m-1)}}{2}\right)T_{(m-1)t+\Delta t} - C_{(m-1)}\left(\frac{\Delta r\, r_o \rho h_m}{2k r_m}\right)\dot{r}_m + \frac{C_{(m-1)}}{2} T_{(m+1)t+\Delta t} = T_{(m-1)t}$$

$$\left(A_m + \frac{B_i}{2}\right)T_{(m-1)t+\Delta t} - B_i\left(\frac{\Delta r\, r_o \rho h_m}{2k r_m}\right)\dot{r}_m + \left(\frac{B_i}{2} + C_m\right)T_{(m+1)t+\Delta t} = T_{m,t}$$

$$\frac{A_{(m+1)}}{2} T_{(m-1)t+\Delta t} - A_{(m+1)}\left(\frac{\Delta r\, r_o \rho h_m}{2k r_m}\right)\dot{r}_m + \left(\frac{A_{(m+1)}}{2} + B_i\right)T_{(m+1)t+\Delta t} + C_{(m+1)} T_{(m+2)t+\Delta t} = T_{(m+1)t}$$

$$A_{(m+2)} T_{(m+1)t+\Delta t} + B_i T_{(m+2)t+\Delta t} + C_{(m+2)} T_{(m+3)t+\Delta t} = T_{(m+2)t}$$

$$\vdots \qquad\qquad \vdots$$

$$A_N T_{(N-1)t+\Delta t} + B_i T_{N,t+\Delta t} + C_N T_{(N+1)t+\Delta t} = T_{N,t}$$

$$\vdots \qquad\qquad \vdots$$

$$A_{bs-1} T_{(bs-2)t+\Delta t} + B_i T_{(bs-1)t+\Delta t} + C_{(bs-1)} T_{bs,t+\Delta t} = T_{(bs-1),t}$$

$$\left(A_{bs} - C_{bs}\right)T_{(bs-1)t+\Delta t} + \left(B_i + 2C_{bs}\right)T_{bs,t+\Delta t} = T_{bs,t}$$

where

$$K_1 = \frac{2\,\Delta t\, K}{\Delta r\, k}$$

$$K_2 = 1 + \frac{2\,\Delta t\, K}{\Delta r^2}$$

$$K_3 = \frac{2\,\Delta t\,K}{\Delta r^2}$$

$$A_i = \Delta t\,K\left(\frac{1}{2r_i\,\Delta r} - \frac{1}{\Delta r^2}\right)$$

$$B_i = K_2$$

$$C_i = -\Delta t\,K\left(\frac{1}{\Delta r^2} + \frac{1}{2r_i\,\Delta r}\right)$$

It is readily recognized that the system of equations could be put into a tridiagonal form were it not for the two equations preceding and following the equation for the melt layer. If the equations are modified and put into a tridiagonal form, their solution can be greatly simplified by using a recursion solution. Consider the equations (m-1), (m), and (m+1) simplified in the following manner for clarity:

$$C_{1(m-1)} + C_{2(m-1)} + C_{3(m-1)} + C_{4(m-1)} = D_{(m-1)}$$

$$0 + C_{2(m)} + C_{3(m)} + C_{4(m)} + 0 = D_{(m)}$$

$$C_{2(m+1)} + C_{3(m+1)} + C_{4(m+1)} + C_{5(m+1)} = D_{(m+1)}$$

The terms that must be eliminated are $C_{4(m-1)}$ and $C_{2(m+1)}$. In order to eliminate the off-diagonal term $C_{4(m-1)}$, each term in equation (m) can be multipled by $C_{4(m-1)}/C_{4(m)}$ and subtracted from each corresponding term in equation (m-1), without changing the value of the matrix. Equation (m-1) will become

$$\left[C_{1(m-1)} - \boxed{0}\frac{C_{4(m-1)}}{C_{4(m)}}\right] + \left[C_{2(m-1)} - C_{2(m)}\frac{C_{4(m-1)}}{C_{4(m)}}\right]\left[C_{3(m-1)} - C_{3(m)}\frac{C_{4(m-1)}}{C_{4(m)}}\right]$$

$$+ \left[C_{4(m-1)} - C_{4(m)}\frac{C_{4(m-1)}}{C_{4(m)}}\right] = D_{(m-1)} - D_{(m)}\frac{C_{4(m-1)}}{C_{4(m)}}$$

which reduces to

$$\left[C_{2(m-1)} - C_{2(m)}\frac{C_{4(m-1)}}{C_{4(m)}}\right] + \left[C_{3(m-1)} - C_{3(m)}\frac{C_{4(m-1)}}{C_{4(m)}}\right] = D_{(m-1)} - D_{(m)}\frac{C_{4(m-1)}}{C_{4(m)}}$$

The same procedure is applied to equation (m+1), and it becomes

$$\left[C_{3(m+1)} - C_{3(m)} \frac{C_{2(m+1)}}{C_{2(m)}}\right] + \left[C_{4(m+1)} - C_{4(m)} \frac{C_{2(m+1)}}{C_{2(m)}}\right] = D_{(m+1)} - D_{(m)} \frac{C_{2(m+1)}}{C_{2(m)}}$$

Now the set of simultaneous equations can be put into a tridiagonal matrix and solved by a simple recursion method. Appendix A gives the details of this procedure.

In the matrix form the equations will be

$$\begin{bmatrix} C_{11} + C_{12} + C_{13} & & & & \\ & C_{22} + C_{23} + C_{24} & & & \\ & & C_{33} + C_{34} + C_{35} & & \\ & & & C_{44} + C_{45} + C_{46} & \\ & & & & \ddots \\ & & & & C_{i,j} + C_{i,j+1} + C_{i,j+2} \end{bmatrix} \begin{bmatrix} \dot{r} \\ T_{1,t+\Delta t} \\ \dot{r}_m \\ T_{(m+1)t+\Delta t} \\ \vdots \\ T_{bs,t+\Delta t} \end{bmatrix} = \begin{bmatrix} D_{o,t} \\ T_{1,t} \\ T_{m,t} \\ T_{(m+1)t} \\ \vdots \\ T_{bs,t} \end{bmatrix}$$

The solution of this set of equations will yield $\dot{r}$, $\dot{r}_m$, and a temperature profile. From $\dot{r}$ and $\dot{r}_m$, the thickness of the melt layer $d_{m,t+\Delta t}$ can be determined as follows:

$$d_{m,t+\Delta t} = d_{m,t} + \left(\dot{r}_m - \dot{r}\right)\Delta t$$

From this equation, a time history of d_m can be plotted.

Determination of Physical Parameters Pertaining to Surface Heat Input

In order to utilize a computer program developed by Marxman and Wooldridge at the Stanford Research Institute, the heat input to the fuel surface, certain parameters, and physical properties must be known. The most important of these parameters are also the most difficult to obtain; and a short discussion on how they were calculated is in order. It happens that the mass transfer number B incorporates most of the needed parameters; B was previously defined as

$$B = \frac{u_e}{u_b}\frac{\Delta h}{h_v}$$

where, from reference 2,

$$\frac{u_b}{u_e} = \frac{\frac{O}{F}\left(\frac{\Delta h}{h_v}\right)}{K_{O,e} + \left(\frac{O}{F} + K_{O,e}\right)\frac{\Delta h}{h_v}}$$

and

$$\Delta H = c_{p,b}T_b - c_{p,f}T_{f,w}$$

$$h_v = h_{v,b} + \frac{K}{1 - K}\left[c_{p,f}\left(T_{f,w} - T_{o,f}\right)\right]$$

where

$\frac{u_e}{u_b}$ ratio of velocity in main stream to that at flame

ΔH sensible enthalpy difference between flame and fuel surface

$\frac{O}{F}$ oxidizer to fuel ratio

$K_{O,e}$ concentration of oxidizer in free stream

K mass fraction of metal or nonvaporizing material

$c_{p,b}$ specific heat of gaseous products at reaction zone

$c_{p,f}$ specific heat of gaseous fuel at wall

T_b flame temperature

$T_{f,w}$ temperature of fuel surface

$T_{f,o}$ ambient temperature of grain

These parameters were obtained by calculations performed at Langley Research Center, from the manufacturers of lithium and fluorine, and from references 14 and 15. The surface temperature was found by experiment to be approximately 1700° F (926° C). (See ref. 13.)

Physical Properties of the Solid Fuel

The pertinent physical parameters of the solid fuel are

k	thermal conductivity state values
ρ	density
c_p	specific heat
h_v	heat of vaporization
h_m	heat of fusion

All the preceding properties, except the thermal conductivity, can easily be obtained from handbooks, tables, and so forth. A method for obtaining the thermal conductivity of a nonhomogeneous substance such as the solid fuel is presented in reference 16. Reference 16 deals with the effects of the addition of metal particles on the thermal conductivity of plastics. In the solid fuel in question, metal particles are added to a hydrocarbon binder; thus, the problems are almost identical. Reference 16 indicates that two-phase systems consisting of powder and gas may be used to give preliminary thermal conductivity data for two-component systems containing plastic and metal particles. The results were given in graphs where the abscissa is the ratio of solid conductivity to gas conductivity and the ordinate is the ratio of effective conductivity to gas conductivity. A third parameter is the fraction of the space occupied by the gas. The thermal conductivity of the solid fuel system can be obtained by making the lithium metal analogous to the solid and letting the hydrocarbon binder be represented by the gas. The fraction of the space occupied by the hydrocarbon can easily be determined. By using this information in the graphs of reference 16, the thermal conductivity of the solid tribrid rocket fuel can be estimated.

Computer Program Analysis

The repetitive solution of a set of 200 to 300 simultaneous equations can prove to be rather time consuming when done manually. For this reason, a computer program was written whereby this same solution can be obtained in a very few minutes. The program is exceptionally easy to use and its use is a matter of supplying a small number of input statements. Typical printouts include: temperature profiles through the grain; the regression rate of the surface RDOTV; the regression rate of the solid-melt interface RDOTM; the thickness of the melt layer DM; and the thickness of the solid layer DS. Any other output can be printed out if the user so desires.

The original computer program was written so that additional elements could be added to the melt layer as it increased and elements subtracted from the solid grain as it decreased. When the program was executed by using this method, it was found that when an element was added or subtracted, the melt-solid regression rate (RDOTM) became unstable and produced an erratic and unsatisfactory time plot for RDOTM. This condition was due to the fact that temperature gradients were changed discontinuously at those times, and the energy balances used in satisfying the boundary conditions were, in turn, made discontinuous. This problem was solved by simply keeping the number of elements in the melt layer and solid grain constant and satisfying the convergence criterion that $\Delta t = \Delta r^2$ for every calculation. Under these conditions the program produces the expected form of time plots of regression rates and temperature profiles.

It appears that the convergence criterion that Δt should be equal to or less than Δr^2 is more than adequate. Comparison of computer runs by using this criterion on Δt and runs using a greater Δt (which is an indication of whether the solution is approaching the exact solution) shows no change in the eighth decimal place. This accuracy is not necessary for engineering purposes. This matter is discussed because the program is taking from 10 to 15 minutes to analyze a 3-inch-thick cylindrical grain. Although this amount of computer time can be tolerated, it could be decreased by an order of magnitude that would be significant.

Appendix B gives the necessary input and a listing of the program and some typical output.

PRESENTATION AND DISCUSSION OF ANALYTICAL RESULTS

The results of this investigation are presented for:

(1) slab burner
(2) cylindrical grain
(3) hypothetical grain

The convective and radiative heat input to the fuel surface with the various fuel compositions was calculated for the cylindrical grain by using a computer program developed by Stanford Research Institute. This information was used as an input for the computer program that was developed as a result of this study. Calculations were made for small laboratory motors with burn times ranging from approximately 20 seconds for fuels with the low-percentage Li grains (70 percent) to 10 seconds for fuels with the high-percentage Li grains (90 percent). For the slab burner an average value of the cylindrical grain heating rates for the same fuel formulation was used. In the case of the hypothetical grain, the heat input that had been calculated for the cylindrical grain was reversed with

respect to time; that is, the heat input that the cylindrical grain was experiencing at the end of burn time was made the heat input to the hypothetical grain at the beginning of burn. The heating rates used in each circumstance, as determined by the Stanford Research Institute program, are shown on the pertinent figures.

Slab Burner

In a slab burner the grain is in rectangular form. It burns with little surface area change, and this situation approximates a condition of constant heat input to the grain surface. Figures 4 show the calculated regression rates of the surface $\dot{r}$ and the solid-melt interface $\dot{r}_m$ as functions of burning time. Note that when $\dot{r}_m$ is larger than $\dot{r}$, the solid-melt interface is receding faster than the surface is vaporizing; therefore, the melt layer will increase in thickness. Figure 4(a) represents a pure lithium grain. Note the relatively large difference between $\dot{r}$ and $\dot{r}_m$ and the fact that in the burning time $\dot{r}$ and $\dot{r}_m$ do not become equal; equal rates would indicate an equilibrium condition. This situation can be improved by mixing the lithium with a low thermal conductivity hydrocarbon fuel, and thus allow less heat to be transferred into the grain to produce the melt layer. When the amount of lithium in the fuel is decreased, the amount of heat generated in the reacting boundary layer is also decreased. Figures 4(b) and 4(c) show the effects that the addition of 10- and 20-percent hydrocarbon binder, respectively, have on the regression-rate curves. It is apparent from these figures that $\dot{r}_m$ can be decreased and equilibrium conditions obtained faster by the addition of a binder.

Figure 5 presents melt-layer thickness as a function of burn time for an 80-percent grain burned at constant heat input to the surface or conditions typical of a slab burner. Note that the melt-layer thickness approaches a constant value in an asymptotic manner. Previous studies by United Technology Center on the other fuel formulations indicate that stripping will occur at a melt thickness of around 0.125 inch (3.17 mm) for laboratory size motors. Figure 6 shows maximum melt-layer thickness as a function of percent lithium for a 3-inch-thick (7.62 cm) grain. Figure 6 gives a percent lithium value of approximately 79 percent at a melt-layer thickness of 0.125 inch (3.17 mm).

Cylindrical Grain

The analysis was extended to a small cylindrical grain rocket motor with an internal diameter of 3 inches (7.62 cm) and an outside diameter of 4.5 inches (11.43 cm). Four fuel formulations were analyzed containing 90, 85, 80, and 70 percent by weight of lithium. The results are shown in figures 7 to 10.

Figures 7 show regression rates for the different fuel formulations as functions of burn time. These curves differ in two very significant ways from the preceding regression rate curves for the slab burner. First, both $\dot{r}_m$ and $\dot{r}$ drop rapidly with time.

Second, the regression rates do not tend to approach each other and therefore never reach an equilibrium condition. Both of these phenomena can be explained by the fact that the heat input to the fuel surface is a function of the inverse of the port area of the motor which increases because of a receding fuel surface and a condition of constant oxidizer flow. The surface regression-rate drop is a direct consequence of decreased heat input per unit area. Because it takes much less energy to melt the fuel than to vaporize it, this condition of decreasing heat input per unit area will have less effect, proportionally, on the melt-solid regression rate than on the surface regression rate; therefore, they will tend not to converge within the reasonable application of cylindrical grains.

Figure 8, which was generated by using surface heat input that was decreasing with time, shows that the melt-layer thickness continually increases with time, and never reaches an equilibrium condition. This condition is the condition experienced in a cylindrical grain at a constant oxidizer flow rate. The melt layer continues to build up at a fairly constant rate and this buildup makes the cylindrical grain most impractical, especially in larger motors that have greater burning time.

Figure 9 is a plot of melt layer at the end of burning as a function of percent lithium in the fuel. As can be seen, even 70-percent lithium has a melt layer that is well above the suggested value of 0.125 inch (3.17 mm).

Figure 10 gives two sets of surface and melt-solid interface regression rates. The reason that two sets of curves were generated is as follows: After the melt layer builds up to a critical depth on the fuel surface, molten fuel droplets will be pulled into the gas stream by viscous forces. The fuel that leaves the surface in this manner will not have absorbed the energy that it would have, had it vaporized. Curves B show the regression rates obtained by assuming that the fuel is vaporized at the surface, and that the heat of vaporization is that energy needed to change the liquid fuel to a gas. Curves A represent the condition of all the molten lithium being injected into the gas stream. Under these conditions an effective heat of gasification of the fuel was calculated where the hydrocarbon binder was decomposed and the lithium was only brought to the surface temperature as a liquid. These two curves represent the limiting condition of the process, and the regression rates should be bracketed by them.

The preceding results indicate that the cylindrical grain will produce more melt layer than the slab burner. High-speed photographs of the slab-burner firings show the occurrence of stripping; therefore, it is apparent that the cylindrical grain will produce even greater melt-layer removal. However, the effectiveness of a downstream turbulator will determine to a large extent the efficiency obtained by a cylindrical motor.

Also, it should be noted that because of an insulated outside boundary condition, the calculations show a melt-layer buildup that proceeds more rapidly toward the end of burning. This condition is due to heat being built up at the insulated wall, and energy that had previously been used to increase the grain temperature will at this point be used to melt the grain. The situation also presented itself in some of the slab burnings, and was noticed in the high-speed photographs that were taken.

Hypothetical Grain

After studying these results, it appears that if the heat input to the surface can be increased as a function of time through manipulation of oxidizer flow rate and grain geometry, the preceding adverse trends could be reversed. In order to verify this theory analytically, computer runs were made where the heat input to the surface was increased with burn time; this procedure is the reverse of the former runs made with the cylindrical grains. It should be made clear that this situation is purely hypothetical. Figures 11 to 13 show the effect that increasing heat input with burn time has on the regression rates. Melt-layer thickness as a function of percent lithium in fuel is shown in figure 12. This plot shows a definite improvement over figure 13. Figure 13 is a plot of melt-layer thickness as a function of burn time for the hypothetical case where the heat input to the surface is increasing with time. This graph shows that the melt layer decreases as the heat transfer increases beyond a certain point. At the point where the $\dot{r}$ curve becomes greater than the $\dot{r}_m$ curve, the melt-layer thickness begins to decrease. It may well be possible to optimize fuel grain design and gas flow characteristics in order to minimize melt-layer buildup. This effect could be of even more importance in large motors where the greater burning time would allow an equilibrium condition to develop.

Influence of Surface Heat Input on Melt-Layer Development

Some important deductions concerning the burning characteristics of a high percentage metal hybrid or tribrid solid fuel can be made from the preceding results. So that a direct comparison of the effect of heat input on the melt layer can be made, a graph of melt-layer thickness as a function of time for the 80-percent lithium fuel for all heat input conditions considered is plotted in figure 14. After analyzing figure 14, the assumption may be made that the melt-layer thickness may be minimized by maximizing the surface heat input, with the reservation that this assumption applies to equilibrium conditions.

CONCLUDING REMARKS

This investigation was undertaken to delineate the effects that an important parameter, fuel thermal conductivity, has on melt-layer buildup and regression rate. An analysis of the results indicates, however, many of the effects of the heat input to the fuel surface from boundary-layer convection and radiation. The original objective was accomplished by producing an analytical method that is dependent upon experimental results for supplying the fuel surface temperature.

The numerical method and mathematical procedure used in this study appear to have performed very satisfactorily. The solution was stable in all computer runs made. The convergence criteria proved to be more than adequate when solutions obtained by using different time increments were compared.

A parabolic temperature profile is obtained rapidly, after a linear temperature profile is initially given to the melt layer and solid grain. The experimental results on regression rates available from slab burner firings agree with the calculations excellently. Motion pictures of the slab-burner firings show melt-layer buildup and the stripping phenomenon as predicted by the calculations.

As expected, the results show a substantial decrease in the melt-layer thickness as the amount of hydrocarbon binder is increased in the tribrid fuel. Also, it was indicated that the surface heat input substantially affects the melt-layer buildup. It is recommended that a study be done to determine to what extent the surface heat input can be controlled in order to minimize the adverse effects of a thick melt layer. The surface heat input is a function of grain geometry and mass flow rates, these among other parameters could possibly be constructively manipulated.

Even though the physical properties for the fuel grain were obtained by using reasonable techniques and assumptions, experimental results would improve the overall accuracy of the method. This statement is especially true of the important parameter thermal conductivity.

It is recommended that this analysis be applied to the problem of determining the aerodynamic and radiative heat input to the fuel surface. Using experimentally determined regression rates and solving one set of equations for heat input would permit this application and would appear to be a possible approach for establishing the validity of our present theories for calculating surface heat input in many types of solid fuel motors.

Langley Research Center,
National Aeronautics and Space Administration,
Langley Station, Hampton, Va., December 2, 1969.

APPENDIX A

SOLUTION OF TRIDIAGONAL SET OF SIMULTANEOUS EQUATIONS

The equations of interest are each of the form

$$A_k T_{k-1} + B_k T_k + C_k T_{k+1} = D_k \qquad (k = 1,2,\ldots K) \qquad (A1)$$

and constitute K equations in the K unknowns $T_1, T_2, \ldots T_k$. This set of equations may be represented by the matrix equation

$$MT = D \qquad (A2)$$

where T is the vector of the unknowns, M is the matrix operator,

$$M \equiv \begin{bmatrix} B_1 & C_1 & 0 & 0 & 0 & \cdots & \cdot & \cdot & \cdot \\ A_2 & B_2 & C_2 & 0 & 0 & \cdots & \cdot & \cdot & \cdot \\ 0 & A_3 & B_3 & C_3 & 0 & \cdots & \cdot & \cdot & \cdot \\ 0 & 0 & A_4 & B_4 & C_4 & \cdots & \cdot & \cdot & \cdot \\ \cdot & \cdot & \cdot & \cdot & \cdot & & \cdot & \cdot & \cdot \\ \cdot & \cdot & \cdot & \cdot & \cdot & \cdots & \cdot & \cdot & \cdot \\ \cdot & \cdot & \cdot & \cdot & \cdot & & \cdot & \cdot & \cdot \\ \cdot & \cdot & \cdot & \cdot & \cdot & \cdots & A_{K-1} & B_{K-1} & C_{K-1} \\ \cdot & \cdot & \cdot & \cdot & \cdot & \cdots & \cdot & A_K & B_K \end{bmatrix} \qquad (A3)$$

and D denotes the resulting matrix.

The matrix M is now factored into two factors L and U; that is,

$$M = LU \qquad (A4)$$

which, because of the tridiagonal form of equation (A3), may be taken in a particularly convenient form of a lower triangular matrix

APPENDIX A

$$L \equiv \begin{bmatrix} w_1 & 0 & & & & \\ u_2 & w_2 & 0 & & & \\ 0 & u_3 & w_3 & 0 & & \\ & & & u_{K-1} & w_{K-1} & 0 \\ & & & & u_K & w_K \end{bmatrix} \tag{A5}$$

and an upper triangular matrix with unit diagonal

$$U \equiv \begin{bmatrix} 1 & v_1 & 0 & & & \\ 0 & 1 & v_2 & 0 & & \\ 0 & 0 & 1 & v_3 & 0 & \\ & & & 0 & 1 & v_{K-2} & 0 \\ & & & & 0 & 1 & v_{K-1} \\ & & & & 0 & 0 & 1 \end{bmatrix} \tag{A6}$$

Formal execution of the operations indicated by equation (A4) leads to the recursion formulas

$$w_1 = B_1 \tag{A7}$$

$$v_1 = \frac{C_1}{w_1} = \frac{C_1}{B_1} \tag{A8}$$

$$w_k = B_k - A_k v_{k-1} \qquad (k = 2,3,\ldots K) \tag{A9}$$

$$v_k = \frac{C_k}{w_k} \qquad (k = 2,3,\ldots K) \tag{A10}$$

$$u_k \equiv A_k \tag{A11}$$

so that the elements of L and U are readily determined.

By definition,

$$g \equiv UT \tag{A12}$$

thus, equations (A2) and (A4) give

$$LUT = Lg = D \tag{A13}$$

Then, by utilizing the lower triangular form of L,

$$g_1 = \frac{D_1}{w_1}$$

$$g_k = \frac{D_k - A_k g_{k-1}}{w_k} \qquad (k = 2,3,\ldots K) \tag{A14}$$

By referring to equation (A12), only the elements of T yet remain and are given by the recursion formula

$$T_K = g_K \tag{A15}$$

$$T_k = g_k - v_k T_{k+1} \qquad (k = K,K-1,\ldots 3,2) \tag{A16}$$

Thus, the unknown temperatures are generated from these equations in the order $T_K, T_{K-1}, \ldots T_1$.

When the elements of the tridiagonal coefficient matrix depend upon the unknown temperatures (as is the case when properties are temperature dependent), an iteration procedure must be adopted in which the most recent value of the calculated temperatures is used in the computation of the elements of the matrix. The solution outlined is repeated successively until the computed temperatures agree within a desired precision.

APPENDIX B

COMPUTER PROGRAM

The necessary input and some appropriate comments are as follows:

RO	inside diameter of a hollow cylindrical grain (inches)
BIGR	outside diameter of a hollow cylindrical grain (inches)
DMZ	initial thickness of the melt layer. This value should be very small, on the order of 0.01 or 0.001 (inches) (0.254 mm or 0.0254 mm)
DELRM	thickness of a finite element in the melt layer. Because of the nature of the equations, there must be at least four elements in the melt layer (inches)
DELRS	thickness of a finite element in the solid grain (inches)
DELT	time increment between calculations. Reference 12 recommends a convergence criterion of $\Delta t \approx \Delta X^2$. This criterion appears to be more than adequate (seconds)
TSURF	surface temperature of grain (^{o}F)
TMELT	melt temperature of grain (^{o}F)
HV	heat of vaporization of the fuel (Btu/lb)
HM	heat of fusion Q of the fuel (Btu/lb)
RHO	density of fuel (lb/in^3)
CP	specific heat of fuel (Btu/lb-^{o}F)
RT	thermal conductivity of fuel (Btu/in-sec-^{o}F)
Q	heat input to fuel surface due to convection and radiation (Btu/in^2-sec)
MO	initial number of elements in melt layer
TPRINT	time increment on Data Printout (seconds)

TCR time at which calculations are to stop (second)

TEMP(1) an initial temperature profile for the grain. The initial profile form is arbitrary in that the proper configuration is rapidly assumed. This array is one-dimensional starting with the first value as the surface temperature and progressing to the back surface temperature

The program listing is as follows:

```
      PROGRAM D2820(INPUT,OUTPUT,TAPE5=INPUT,TAPE6=OUTPUT)
      REAL KD,KT,K1,K2,K3
      INTEGER S
      DIMENSION R(300),A(300),C(300),DIAG1(300),DIAG2(300),DIAG3(300),
     1ELIM(300),D(300),TEMP(300),IDENT(8)
     2,G(300),W(300),V(300),SAVET(300)
      DIMENSION  QTAB(100),ROTAB(100)
      EQUIVALENCE (R(1),W(1)),(A(1),V(1)),(C(1),G(1))
      NAMELIST/INPUT/RHO,HV,HM,KT,CP,RO,TMELT,TEMP,TSURF,BIGR,DMZ
     1,DELRM,DELT,DELRS,MO,KO,TPRINT,Q,TCR,NQR,QTAB,ROTAB
 3000 READ(5,700)IDENT
      IF (EOF,5) 201,300
  201 STOP
  700 FORMAT(8A10)
  300 WRITE (6,701) IDENT
  701 FORMAT(1H1,8A10//)
      READ(5,INPUT)
      WRITE(6,INPUT)
C
C       COMPUTE INITIAL CONDITIONS
      ICHECK=0
      IERR=0
      KD=KT/(RHO*CP)
      DM=DMZ
      TIME=0.0
      CHANM=0.0
      CHANS=0.0
      M=MO
      XM=M
      XTIME=TIME
      DS=(BIGR-RO)-DM
      K=(DM/DELRM)+(DS/DELRS)
      S=K-M
      RM=RO+DM
      GO TO 1000
C
C     MAIN PROGRAM LOOP
 2000 RO=RO+RDOTV*DELT
      CALL FTLUP (RO,Q,1,NQR,ROTAB,QTAB)
      TIME=TIME+DELT
      IF(TIME.GT.TCR)GO TO 3000
      DM=DM+(RDOTM-RDOTV)*DELT
      RM=RM+(RDOTM*DELT)
      IF(RO.GT.BIGR)GO TO 200
C
C     COMPUTE NEW DELRM
```

APPENDIX B

```
C
      DO 45 I=1,K
   45 SAVET(I)=TEMP(I)
      QUANT=(RDOTM-RDOTV)*DELT
      CHANM=CHANM+QUANT
      IF (CHANM.LT.1000.) GO TO 50
C CHANGE THE NO. OF BOLCKS IN MELT LAYER WHEN THE THICKNESS HAS CHANGED .01
C ADD 1 BLOCK FOR EVERY .01 ADDITION
C GET NEW TEMPERATURE PROFILE IN MELT LAYER
      MOLD=M
      CHANMA=CHANM/.05
      NEWBLK=CHANMA
      XM=XM+CHANMA
      M=XM
      CHANM=0.0
      ANEW=NEWBLK+1
      DIFF = (TEMP(MOLD-1) - TMELT) /ANEW
      DO 46 I=1,NEWBLK
      AI=I
   46 TEMP(M-I) = TMELT+AI*DIFF
      K=M+S
      MP1=M+1
      II=0
      DO 47 I=MP1,K
      II=II+1
   47 TEMP(I)=SAVET(MOLD+II)
      ICHECK=ICHECK+1
      IF (ICHECK.GT.10)GO TO 50
  144 WRITE (6,145) (SAVET(I),I=1,K)
      WRITE (6,147) M,MOLD,NEWBLK,CHANMA,CHANM,DM,RM,RDOTM,RDOTV,TMELT
     1,K,DS,S,CHANS
      WRITE (6,146) (TEMP(I),I=1,K)
  145 FORMAT (*0SAVET*/(7E18.7))
  146 FORMAT (*0TEMP*/(7E18.4))
  147 FORMAT (*0M=*I5,3X,*MOLD=*I5,3X,*NEWBLD=*I5,3X,*CHANMA=*E14.6,3X
     1*CHANM=*E14.6,3X,*DM=*E14.6/ * RM=*E14.6,3X,*RDOTM=*E14.6,3X*RDOTV
     2=*E14.6,3X,*TMELT=*E14.6,3X,*K=I*I5,3X,*DS=*E14.6,3X,*S=*I5/* CHAN
     3S=*E14.6)
   50 DELRM=DM/FLOAT(M-1)
C
C      COMPUTE DELRS
C
      DS=BIGR-RM
      IF ((DS.LT. .1) .OR. (DM.LT. .005)) GO TO 8000
      X=RDOTM*DELT
```

APPENDIX B

```
      CHANS=CHANS+X
      IF (CHANS. LT.1000.)GO TO 80
C CHANGE NO. OF BLOCKS IN SOLID WHEN THICKNESS HAS CHANGED .01
C SUBTRACT 1 BLOCK FOR EVERY .01 CHANGE
C REMOVE BLOCK (MELT-1)
      CHANSA=CHANS/.05
      NCHANSA=CHANSA
      S=S-NCHANSA
      CHANS=0.0
      K=M+S
      MP1=M+1
      IF (ICHECK.GT.3) GO TO 80
      WRITE (6,145) (SAVET(I),I=1,K)
      WRITE (6,146) M,MOLD,NEWBLK,CHANMA,CHANM,DM,RM,RDOTM,RDOTV,TMELT
     1,K,DS,S,CHANS
      WRITE (6,147) (TEMP(I),I=1,K)
   80 DELRS=DS/FLOAT(S)
      K=M+S
      IF (K-300) 90,85,85
   85 WRITE (6,86) M,S,DELT,CHANM,DS,CHANS
      RO=BIGR+1.0
   86 FORMAT (*0NUMBER OF BLOCKS EXCEEDS DIMENSIONS*/* M=*I5,3X*S=*I5,
     13X*DELT=*E15.6,3X*CHANM=*E15.6,3X*DS=*E15.6,3X*CHANS=*E15.6)
       GO TO 40
   90 DELT= DELRM**2
      IF (DELRM.GT.DELRS) DELT= DELRS**2
 1000 DO 2 I=1,M
      R(I)=RO+FLOAT(I)*DELRM
      A(I)=DELT*KD*((1./(2.*R(I)*DELRM))-(1./DELRM**2))
    2 C(I)=-DELT*KD*((1./(2.*R(I)*DELRM))+(1./DELRM**2))
      IF(DS.LT. .001)GO TO 5000
      MP=M+1
      DO 3 I=MP,K
      R(I)=RM+FLOAT(I-M)*DELRS
      A(I)=DELT*KD*((1./(2.*R(I)*DELRS))-(1./DELRS**2))
    3 C(I)=-DELT*KD*((1./(2.*R(I)*DELRS))+(1./DELRS**2))
C
C     COMPUTE DIAGONALS OF MATRIX
C
 5000 K1=(2.*DELT*KD)/(DELRM*KT)
      K2=1.+(2.*DELT*KD)/DELRM**2
      K3=(2.*DELT*KD)/DELRM**2
      DIAG2(1)=-(RHO*HV*K1)/(K2-1.)
      DIAG3(1)=K3/(K2-1.)
      DIAG1(2)=0.
```

APPENDIX B

```
      DIAG2(2)=K2
      DIAG3(2)=C(1)
      MM=M-2
      DO 4 I=3,MM
      DIAG1(I)=A(I-1)
      DIAG2(I)=K2
      DIAG3(I)=C(I-1)
    4 CONTINUE
      IF(DS.LT. .001)GO TO 6000
      DIAG1(M-1)=A(M-2)
      DIAG2(M-1)=K2+C(M-2)/2.
      DIAG3(M-1)=-C(M-2)*((DELRM*RO*RHO*HM)/(2.*KT*RM))
      EXTRAR=C(M-2)/2.
      DIAG1(M)=A(M-1)+(K2/2.)
      DIAG2(M)=-K2*((DELRM*RO*RHO*HM)/(2.*KT*RM))
      DIAG3(M)=(K2/2.)+C(M-1)
      B=1.+(2.*DELT*KD)/DELRS**2
      EXTRAL=(A(M)/2.)
      DIAG1(M+1)=-A(M)*((DELRM*RO*RHO*HM)/(2.*KT*RM  ))
      DIAG2(M+1)=(A(M)/2.)+K2
      DIAG3(M+1)=C(M)
      M2=M+2
      KM1=K-1
      DO 5 I=M2,KM1
      DIAG1(I)=A(I-1)
      DIAG2(I)=B
      DIAG3(I)=C(I-1)
    5 CONTINUE
 6000 IF(DS.LT.  .001)K=M-1
      DIAG1(K)=A(K-1)
      DIAG2(K)=B+C(K-1)
      DIAG3(K)=0.0
C
C     COMPUTE COLUMN VECTOR
C
      D(1)=TSURF-(K1/(K2-1.))*Q
      D(2)=TEMP(2)-A(1)*TSURF
      DO 7 I=3,K
    7 D(I)=TEMP(I)
      IF(DS.LT.  .001)GO TO 7000
      D(M)=TMELT
      D(M-1)=D(M-1)-D(M)*EXTRAR/DIAG3(M)
      D(M+1)=D(M+1)-D(M)*EXTRAL/DIAG1(M)
C
C     PUT MATRIX INTO TRI-DIAGONAL FORM BY ELIMINATING OFF DIAGONAL TERMS
```

APPENDIX B

```
C
      DIAG3(M-1)=DIAG3(M-1)-(DIAG2(M)*EXTRAR)/DIAG3(M)
      DIAG2(M-1)=DIAG2(M-1)-(DIAG1(M)*EXTRAR)/DIAG3(M)
      DIAG1(M+1)=DIAG1(M+1)-(DIAG2(M)*EXTRAL)/DIAG1(M)
      DIAG2(M+1)=DIAG2(M+1)-(DIAG3(M)*EXTRAL)/DIAG1(M)
C
C     TRI-DIAGONAL MATRIX SOLUTION
C
 7000 W(1)=DIAG2(1)
      V(1)=DIAG3(1)/W(1)
      G(1)=D(1)/W(1)
      DO 20 JJ=2,K
      W(JJ)=DIAG2(JJ)-DIAG1(JJ)*V(JJ-1)
      V(JJ)=DIAG3(JJ)/W(JJ)
   20 G(JJ)=(D(JJ)-DIAG1(JJ)*G(JJ-1))/W(JJ)
      KM=K-1
      TEMP(K)=G(K)
      DO 30 JJ=1,KM
   30 TEMP(K-JJ)=G(K-JJ)-V(K-JJ)*TEMP(K-JJ+1)
      RDOTV=TEMP(1)
      IF(RDOTV.LT.0.0)RDOTV=0.0
      RDOTM=TEMP(M)
      IF(TIME.EQ.0.)GO TO 2020
      IF((TIME-XTIME).LT. TPRINT)GO TO 2030
      XTIME=TIME
 2020 CONTINUE
   40 WRITE (6,705) TIME
  705 FORMAT (*0TIME=*E15.8/*0TEMPERATURES*)
      WRITE(6,702)(TEMP(JJ),JJ=1,K)
  702 FORMAT(5(5X,E15.8))
      WRITE (6,704 ) RM,DM, DS,DELRS,RDOTV,RDOTM,DELRM,RO
  704 FORMAT (*0    RM=*E15.8,5X,*    DM=*E15.8,5X,*    DS=*E15.8,5X,*    DE
     1LRS=*E15.8/* RDOTV=*E15.8,5X,*RDOTM=*E15.8,5X,*DELRM=*E15.8,5X,*RO
     2=*E15.8)
      WRITE(6,810)
  810 FORMAT(/*  D ARRAY*/)
      WRITE(6,702)(D(JJ),JJ=1,K)
      IF(IERR.NE.0) GO TO 3000
 2030 CONTINUE
      GO TO 2000
  200 CONTINUE
      WRITE(6,703)
  703 FORMAT(23H DM GREATER THAN (R-RO))
      GO TO 3000
 8000 IERR=1
      GO TO 40
      END
```

```
TIME= 2.50011347E+00

TEMPERATURES
     2.06588970E-01      1.18297415E+03      7.66369910E+02      2.08171915E-01      2.30713472E+02
     1.11436173E+02      1.00539992E+02      1.00017356E+02      1.00000422E+02      1.00000008E+02
     1.00000000E+02      1.00000000E+02      1.00000000E+02

   RM= 3.62418308E+00        DM= 1.09950680E-02        DS= 8.75816923E-01        DELRS= 9.73129914E-02
RDOTV= 2.06588970E-01     RDOTM= 2.08171915E-01     DELRM= 3.66502266E-03     RO= 3.61318801E+00

 D ARRAY

    -3.63252056E+03      1.18397993E+03      7.66590147E+02      3.50000000E+02      2.30933439E+02
     1.11436078E+02      1.00539983E+02      1.00017356E+02      1.00000422E+02      1.00000008E+02
     1.00000000E+02      1.00000000E+02      1.00000000E+02

TIME= 2.60012092E+00

TEMPERATURES
     2.03833209E-01      1.18297056E+03      7.66366397E+02      2.05443101E-01      2.31071840E+02
     1.12158601E+02      1.00611547E+02      1.00020966E+02      1.00000544E+02      1.00000011E+02
     1.00000000E+02      1.00000000E+02      1.00000000E+02

   RM= 3.64486507E+00        DM= 1.11547161E-02        DS= 8.55134930E-01        DELRS= 9.50149922E-02
RDOTV= 2.03833209E-01     RDOTM= 2.05443101E-01     DELRM= 3.71823869E-03     RO= 3.63371035E+00

 D ARRAY

    -3.63727678E+03      1.18397634E+03      7.66586636E+02      3.50000000E+02      2.31291803E+02
     1.12158499E+02      1.00611537E+02      1.00020966E+02      1.00000544E+02      1.00000011E+02
     1.00000000E+02      1.00000000E+02      1.00000000E+02

TIME= 2.70012589E+00

TEMPERATURES
     2.01114651E-01      1.18296688E+03      7.66362799E+02      2.02752151E-01      2.31444267E+02
     1.12909520E+02      1.00690800E+02      1.00025232E+02      1.00000698E+02      1.00000016E+02
     1.00000000E+02      1.00000000E+02      1.00000000E+02

   RM= 3.66527555E+00        DM= 1.13170879E-02        DS= 8.34724448E-01        DELRS= 9.27471609E-02
RDOTV= 2.01114651E-01     RDOTM= 2.02752151E-01     DELRM= 3.77236262E-03     RO= 3.65395846E+00

 D ARRAY

    -3.64222134E+03      1.18397265E+03      7.66583039E+02      3.50000000E+02      2.31664225E+02
     1.12909411E+02      1.00690788E+02      1.00025231E+02      1.00000698E+02      1.00000016E+02
     1.00000000E+02      1.00000000E+02      1.00000000E+02
```

REFERENCES

1. Muzzy, R. J.: Schlieren and Shadowgraph Studies of Hybrid Boundary-Layer Combustion. AIAA J., vol. 1, no. 9, Sept. 1963, pp. 2159-2160.

2. Marxman, G. A.; Wooldridge, C. E.; and Muzzy, R. J.: Fundamentals of Hybrid Boundary-Layer Combustion. Progress in Astronautics and Aeronautics, Vol. 15, Academic Press, Inc., c.1964, pp. 485-522.

3. Marxman, G. A.; and Wooldridge, C. E.: Research on the Combustion Mechanism of Hybrid Rockets. Advances in Tactical Rocket Propulsion, AGARD CP No. 1, c.Aug. 1968, pp. 421-478.

4. Schlichting, Hermann (J. Kestin, trans.): Boundary Layer Theory. Fourth ed., McGraw Hill Book Co., Inc., c.1960.

5. Mager, Artur: Transformation of the Compressible Turbulent Boundary Layer. J. Aeron. Sci., vol. 25, no. 5, May 1958, pp. 305-311.

6. Burggraf, O. R.: The Compressibility Transformation and the Turbulent-Boundary-Layer Equations. J. Aerosp. Sci., vol. 29, no. 4, Apr. 1962, pp. 434-439.

7. Crocco, L.: Transformations of the Compressible Turbulent Boundary Layer With Heat Exchange. AIAA J., vol. 1, no. 12, Dec. 1963, pp. 2723-2731.

8. Marxman, Gerald A.: Combustion in the Turbulent Boundary Layer on a Vaporizing Surface. Tenth Symposium (International) on Combustion, Combustion Inst., 1965, pp. 1337-1349.

9. Wooldridge, C. E.; and Muzzy, R. J.: Measurements in a Turbulent Boundary Layer With Porous Wall Injection and Combustion. Tenth Symposium (International) on Combustion, Combustion Inst., 1965, pp. 1351-1362.

10. Mickley, H. S.; and Davis, R. S.: Momentum Transfer for Flow Over a Flat Plate With Blowing. NACA TN 4017, 1957.

11. Carslaw, H. S.; and Jaeger, J. C.: Conduction of Heat in Solids. First ed., The Clarendon Press (Oxford), 1947.

12. Gay, B.; and Cameron, P. T.: The Efficiency of Numerical Solutions of the Heat-Conduction Equation. Paper No. 67-WA/HT-17, Amer. Soc. Mech. Eng., 1967.

13. O' Brien, George G.; Hyman, Morton A.; and Kaplan, Sidney: A Study of the Numerical Solution of Partial Differential Equations. J. Math. Phys., vol. XXIX, no. 4, Jan. 1951, pp. 223-251.

14. Arbit, H. A.; Dickerson, R. A.; Clapp, S. D.; and Nagai, C. K.: Lithium-Fluorine-Hydrogen Propellant Study. NASA CR-72325, 1968.

15. Anon.: A Compendium of Data on Lithium and Selected Compounds of Lithium. Lithium Corp. America, Inc., Feb. 1958. (Revised July 1959.)

16. Franzen, Marvin H.: The Effects of the Addition of Metal Particles on the Thermal Conductivity of Plastic. M.S. Thesis, U.S. Air Force Inst. Technol., 1958.

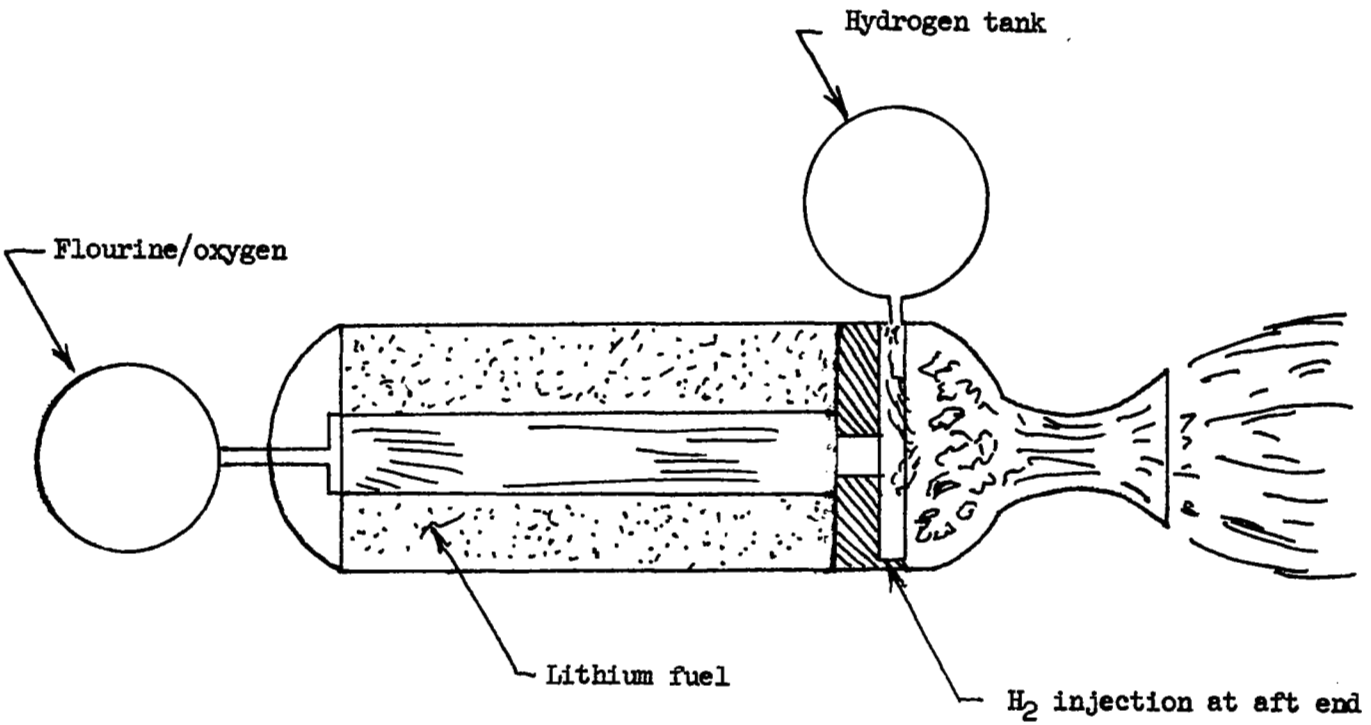

Figure 1.- Tribrid rocket system.

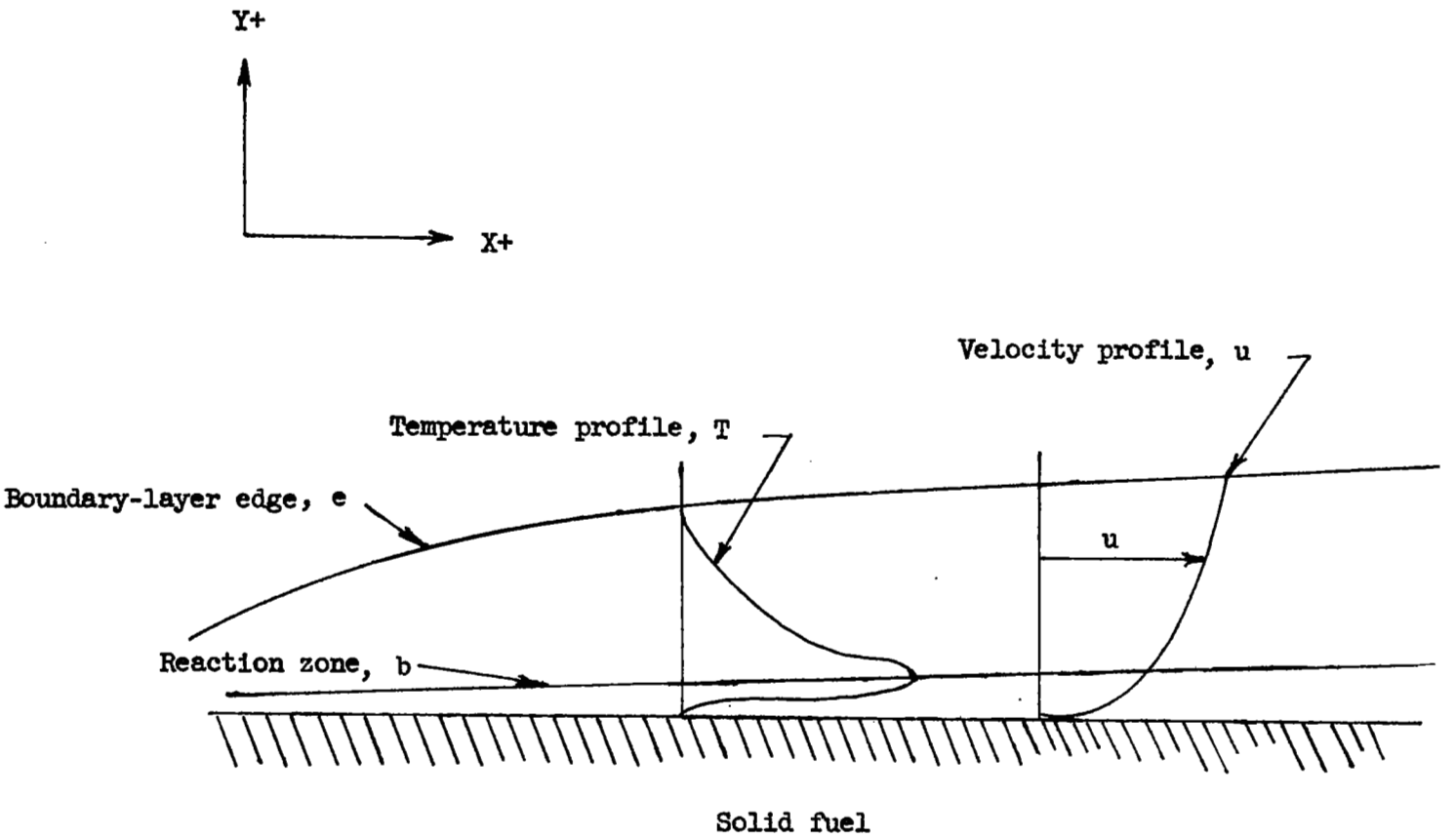

Figure 2.- Reacting boundary layer.

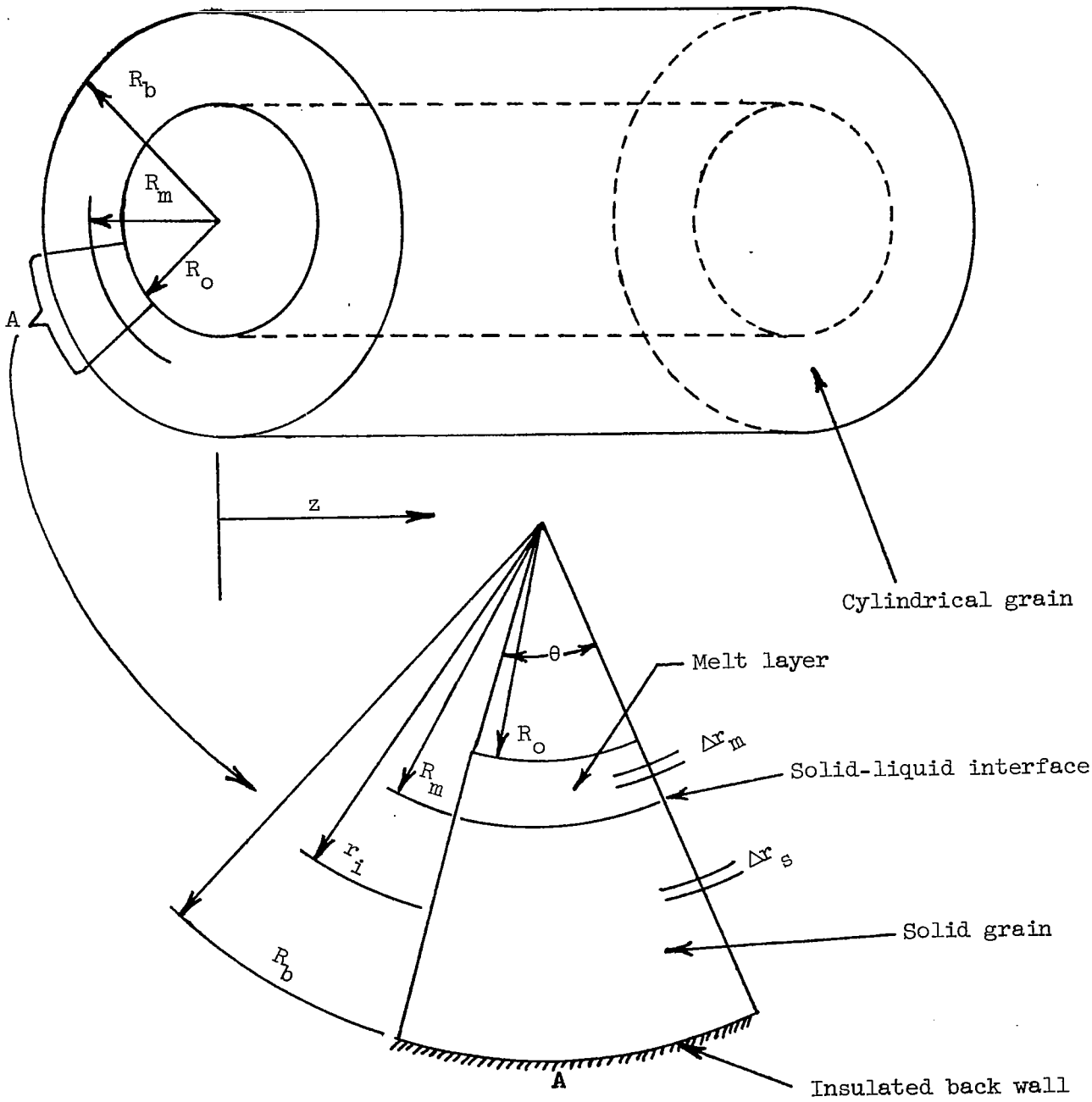

Figure 3.- Cross section of tribrid fuel grain.

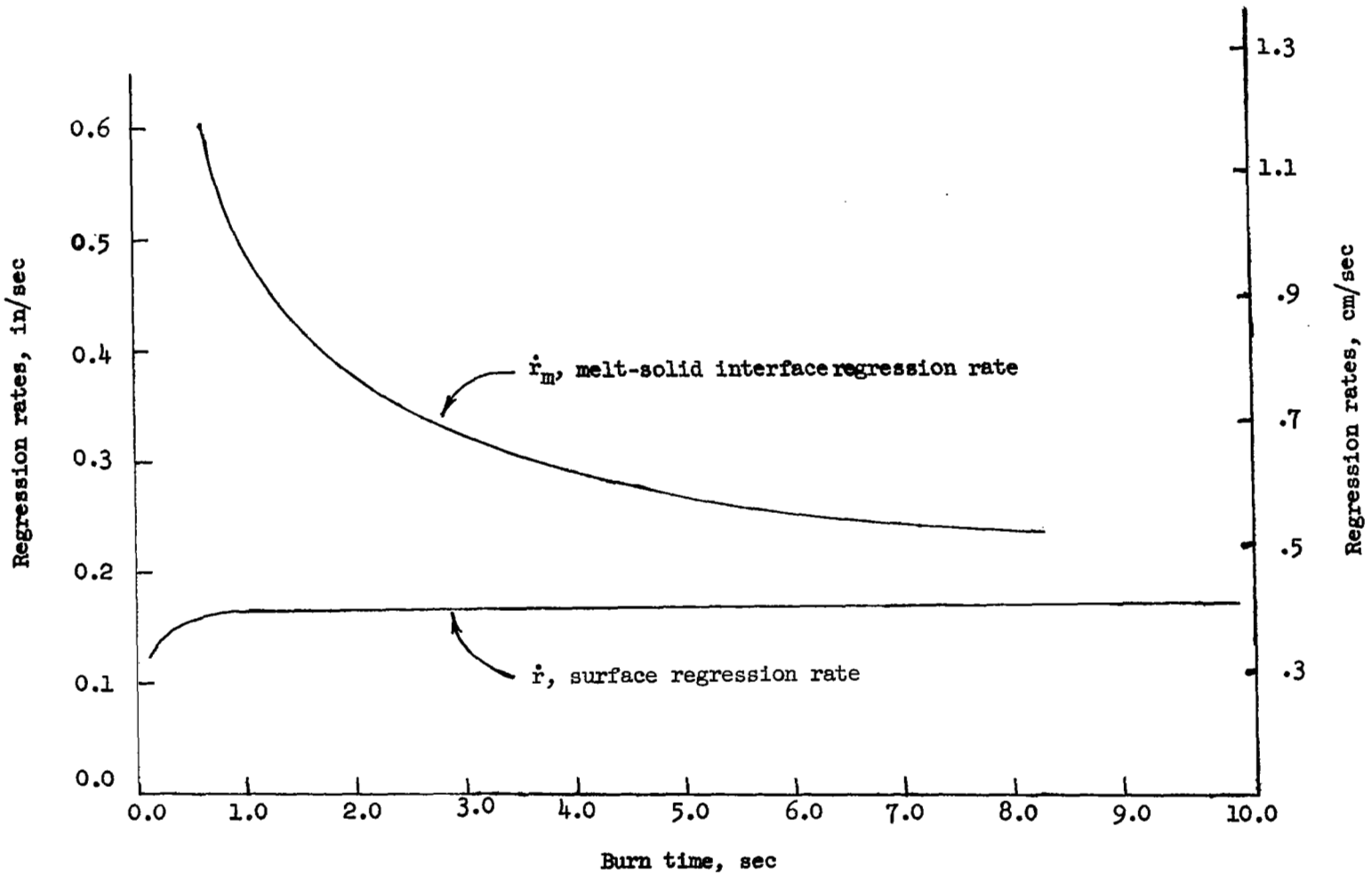

(a) Pure lithium grain; heat imput to surface is equal to 26 Btu/in^2-sec $(42.48 \times 10^6$ W/m$^2)$.

Figure 4.- Regression rates as functions of burn time for slab burner.

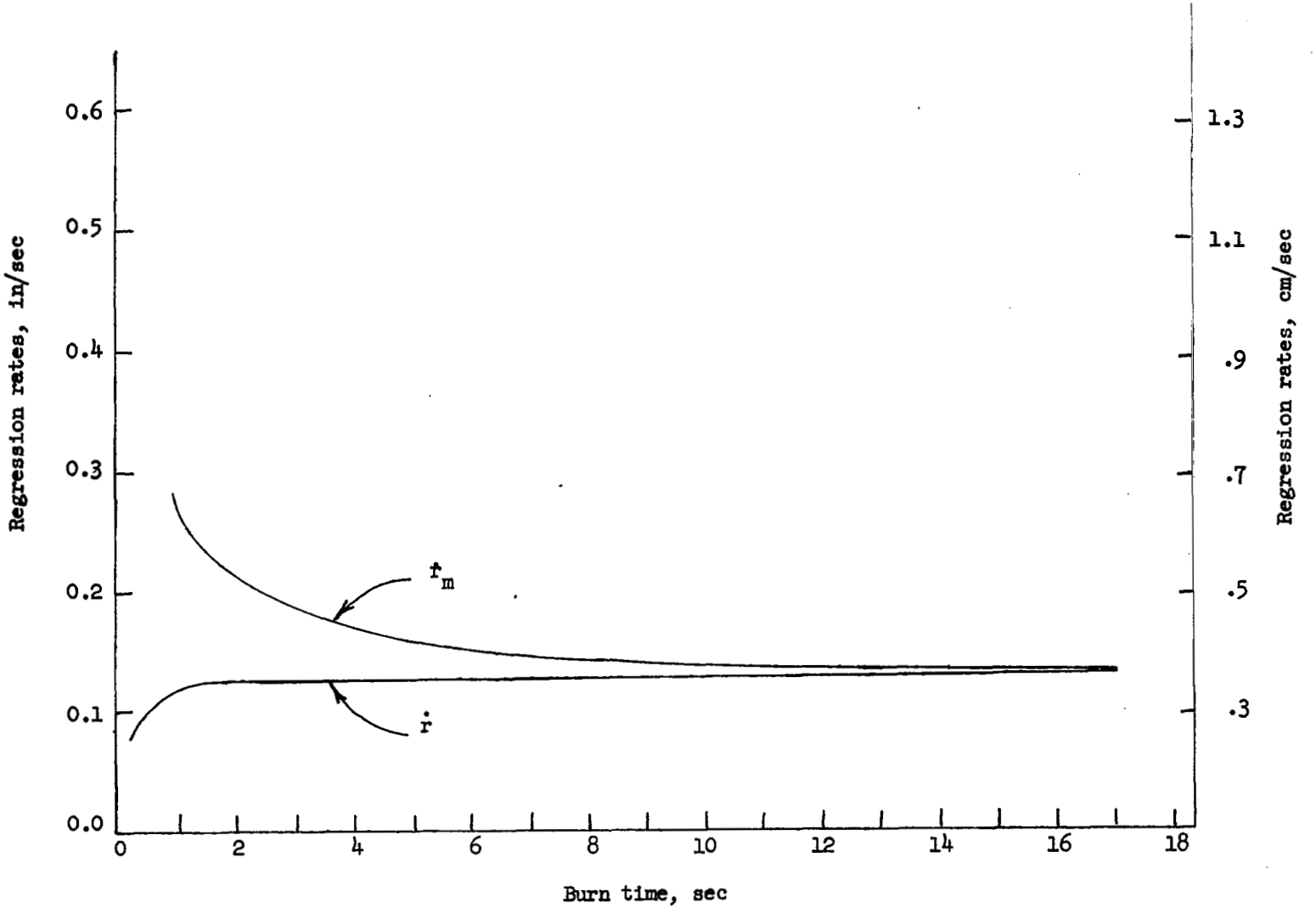

(b) 90-percent-lithium—10-percent binder grain; heat imput to surface is equal to 20 Btu/in^2-sec $(32.68 \times 10^6$ W/m$^2)$.

Figure 4.- Continued.

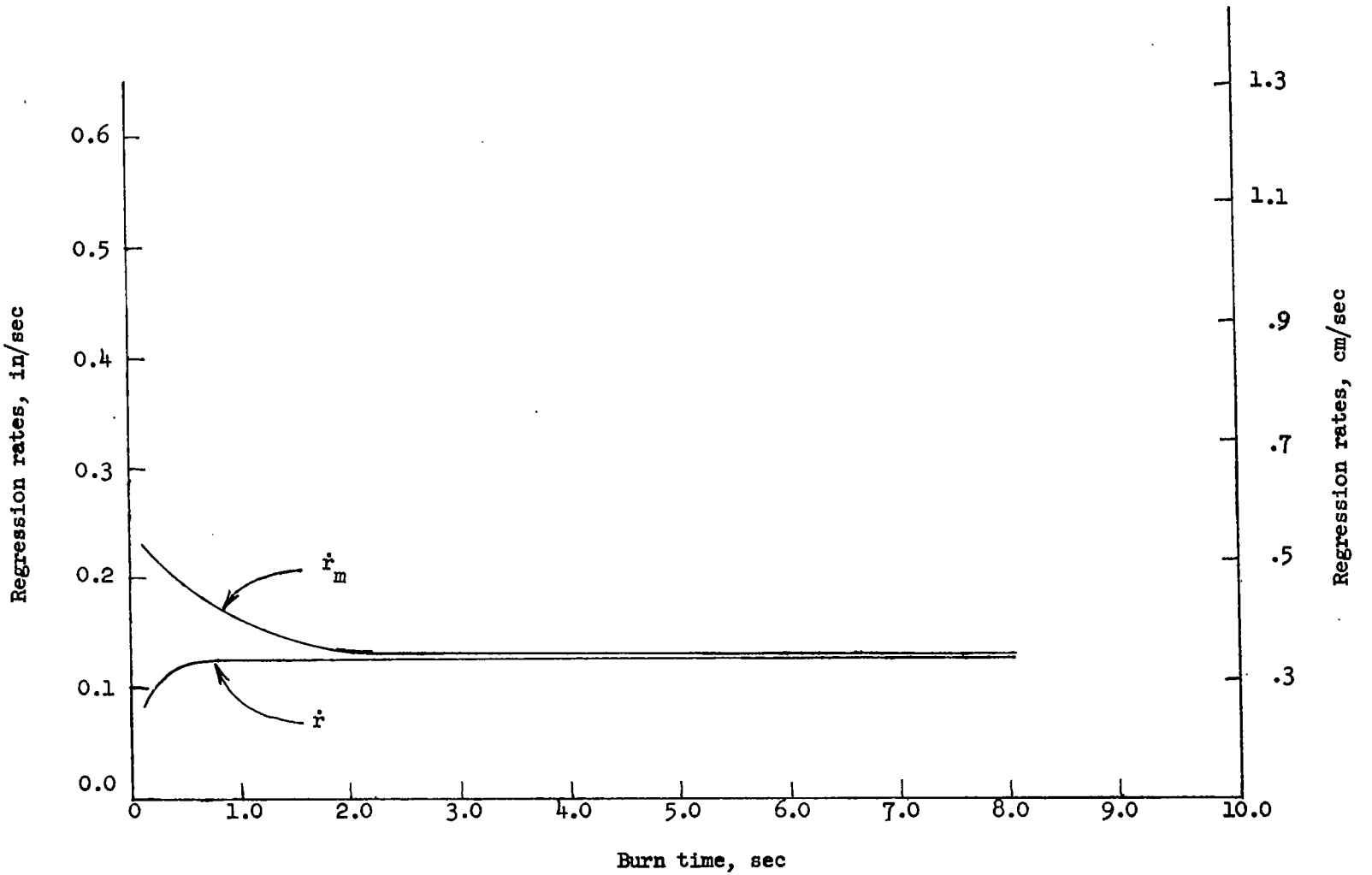

(c) 80-percent-lithium–20-percent-binder grain; heat imput to surface is equal to 15 Btu/in^2-sec (24.51 W/m^2).

Figure 4.- Concluded.

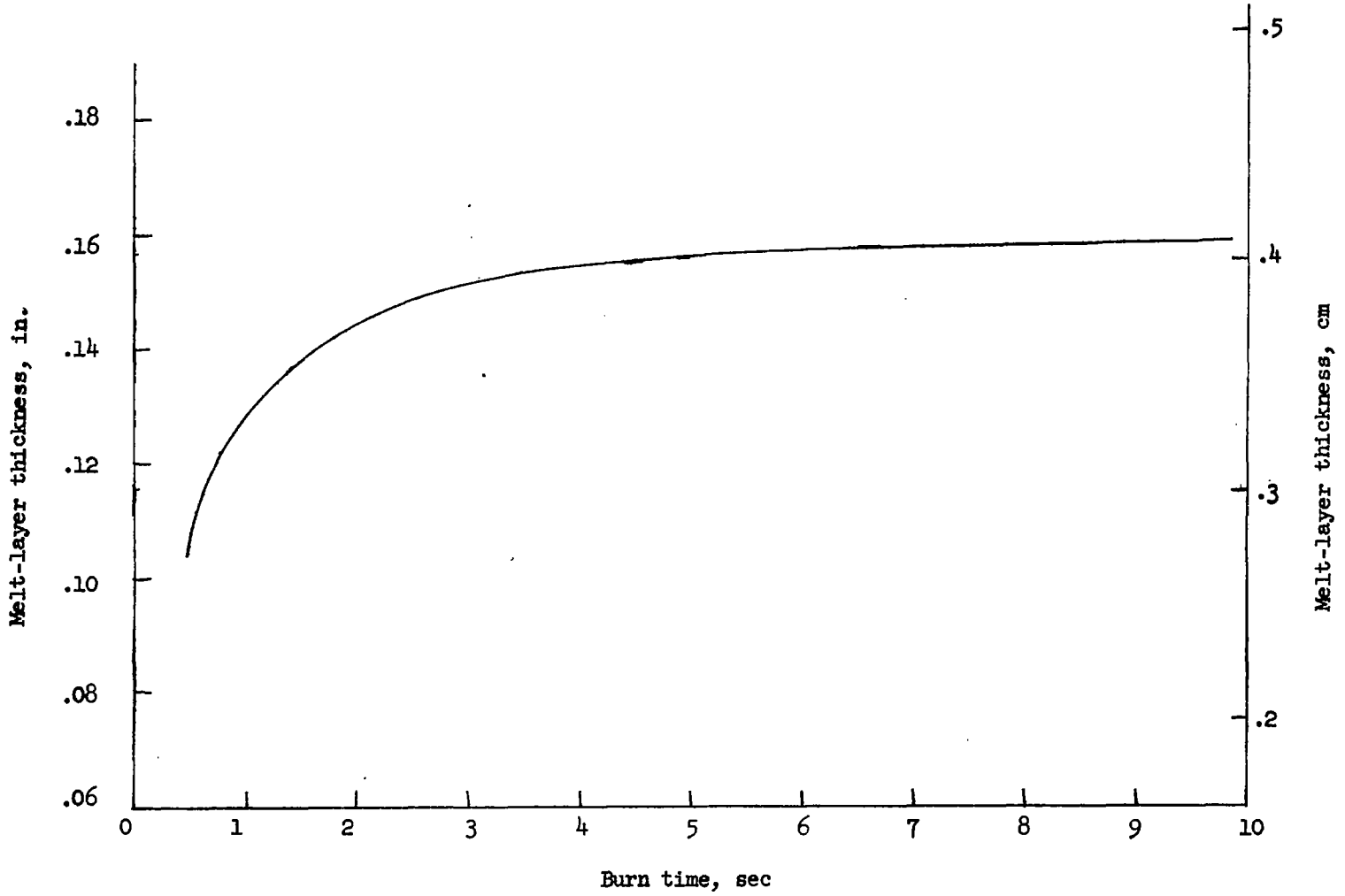

Figure 5.- Melt-layer thickness as function of burn time. Slab burner; constant heat input to fuel surface; 80-percent-lithium--20-percent binder.

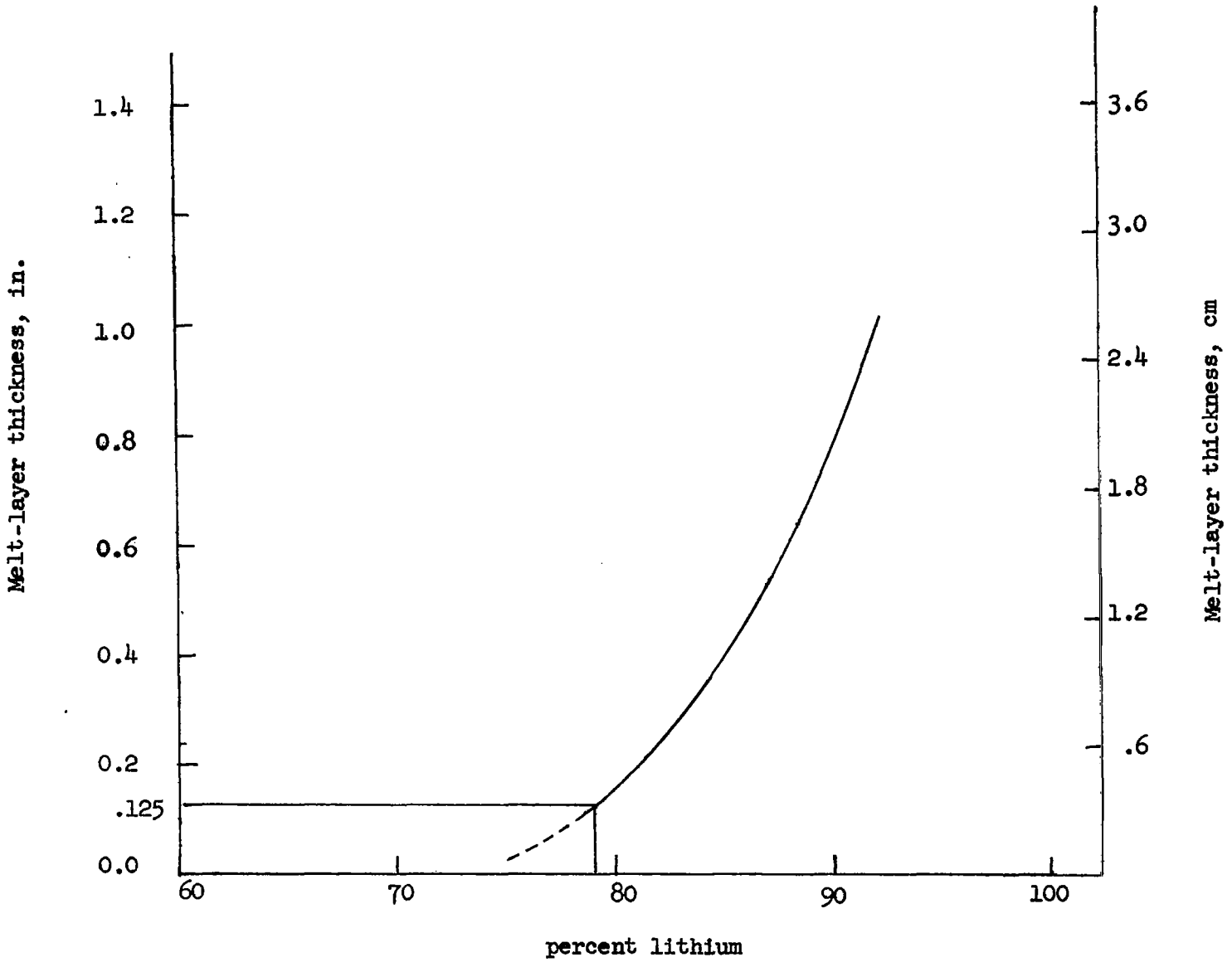

Figure 6.- Maximum melt-layer thickness as function of percent lithium. Slab burner; constant heat input to fuel surface.

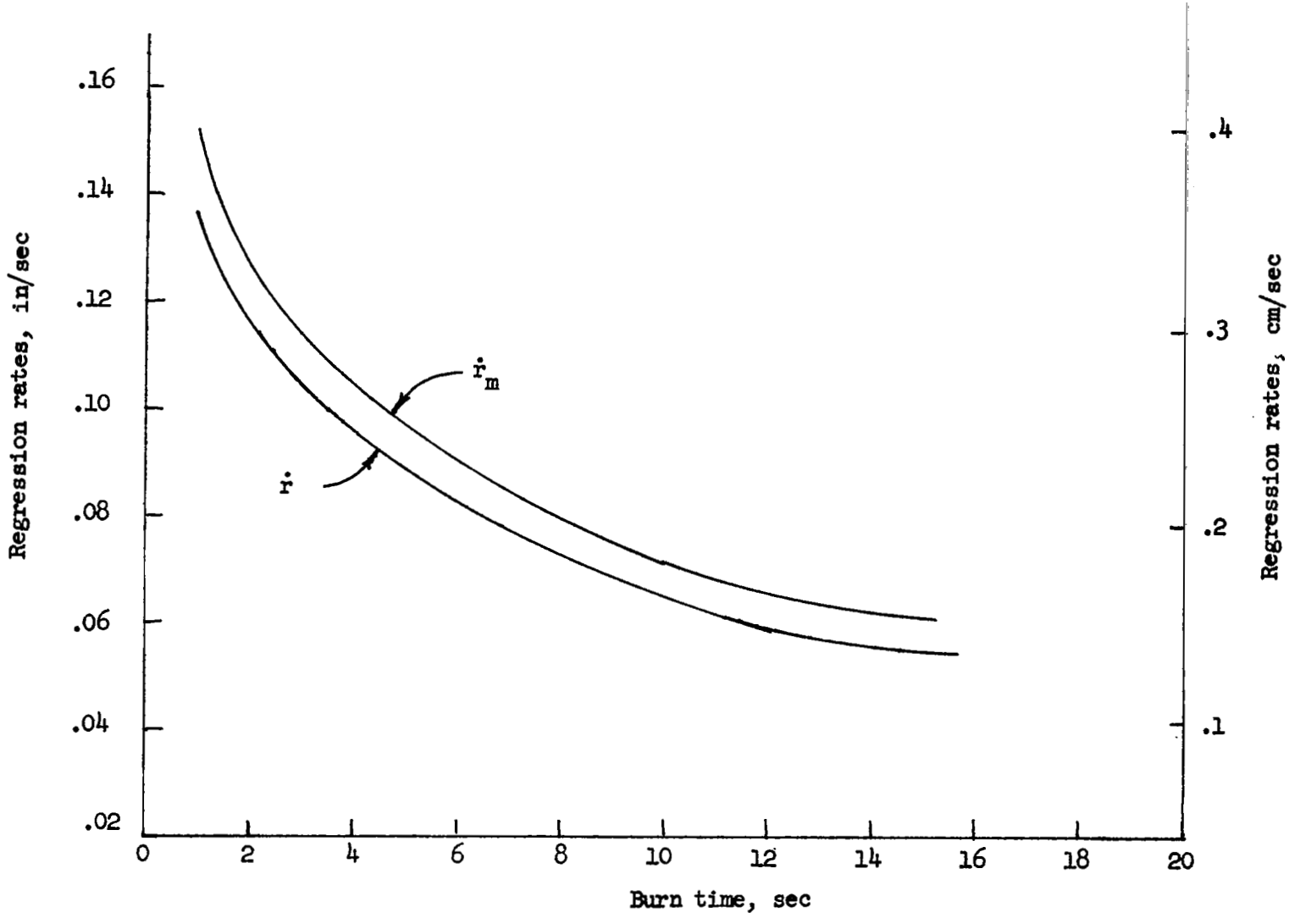

(a) 70-percent-lithium—30-percent-binder; heat input to surface; $\dot{Q}$ = 12.7 Btu/in^2-sec $(20.75 \times 10^6$ W/m$^2)$ at burn time = 0; $\dot{Q}$ = 3.85 Btu/in^2-sec $(6.29 \times 10^6$ W/m$^2)$ at burnout.

Figure 7.- Regression rates as function of burn time. Cylindrical grain.

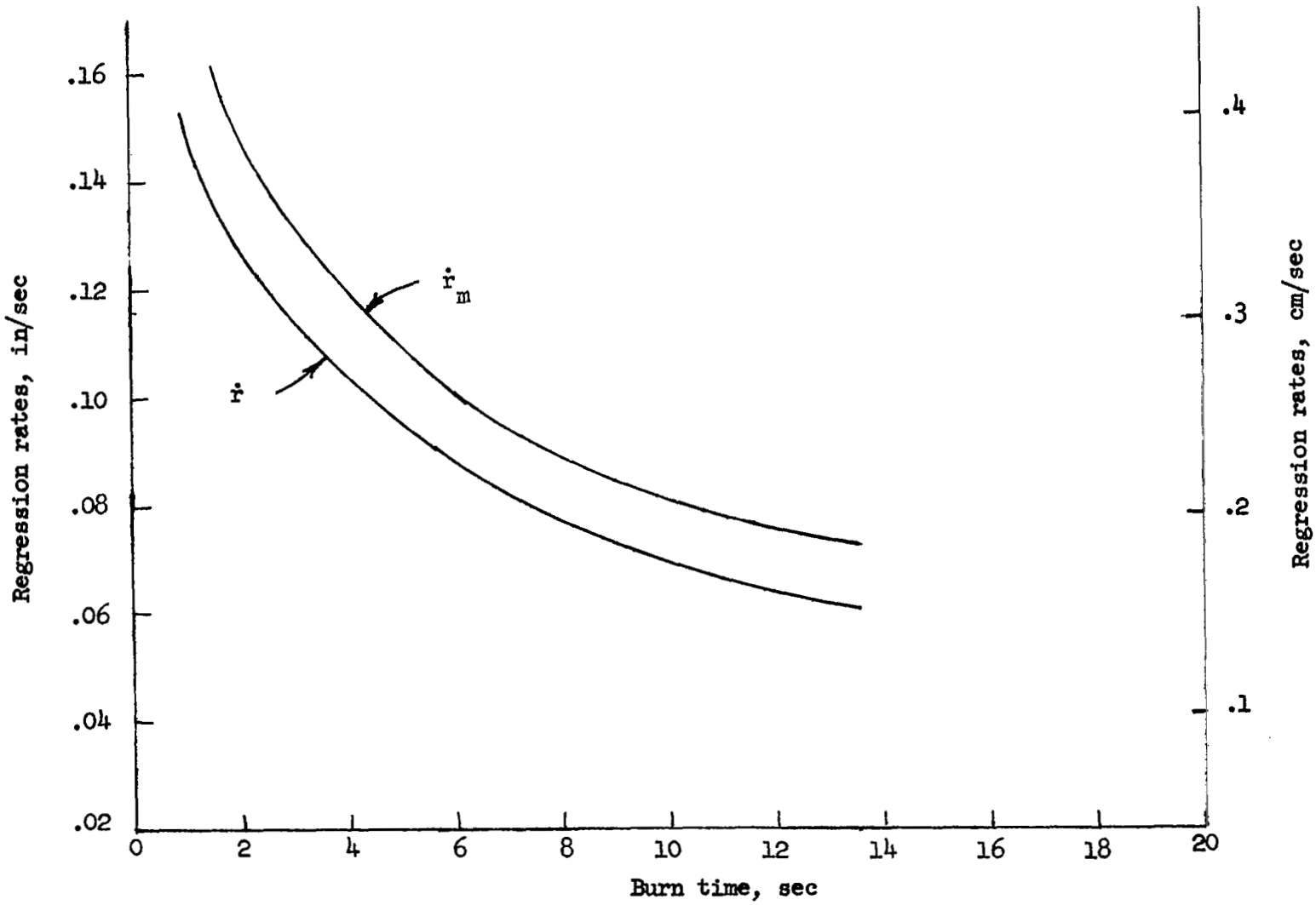

(b) 80-percent-lithium—20-percent-binder; $\dot{Q}$ = 20 Btu/in^2-sec $(32.68 \times 10^6$ W/m$^2)$ at time = 0; $\dot{Q}$ = 6 Btu/in^2-sec $(9.8 \times 10^6$ W/m$^2)$ at burnout.

Figure 7.- Continued.

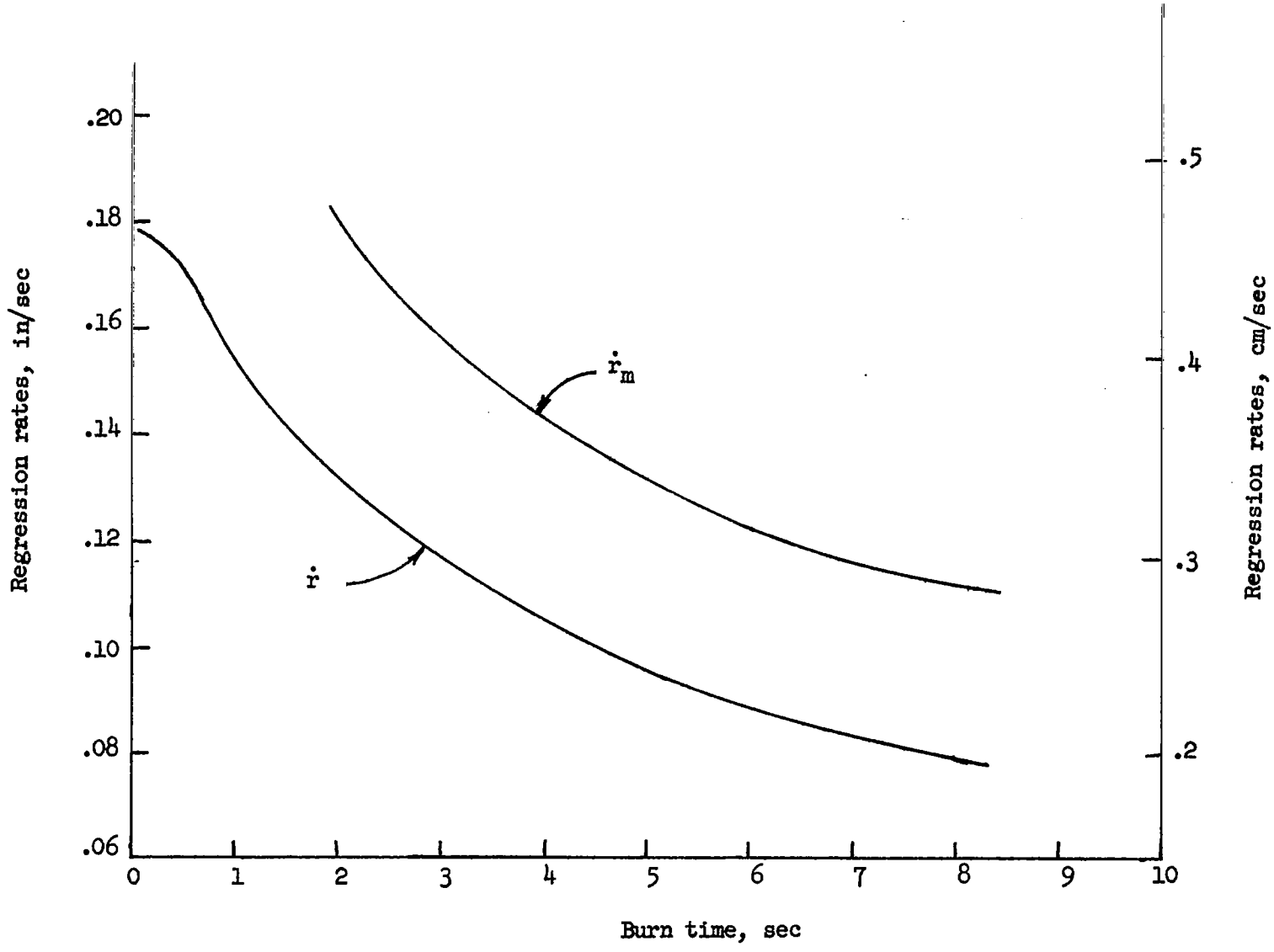

(c) 85-percent-lithium—15-percent-binder; $\dot{Q}$ = 28 Btu/in^2-sec $(45.75 \times 10^6$ W/m$^2)$ at time = 0; $\dot{Q}$ = 8.5 Btu/in^2-sec $(13.89 \times 10^6$ W/m$^2)$ at burnout.

Figure 7.- Continued.

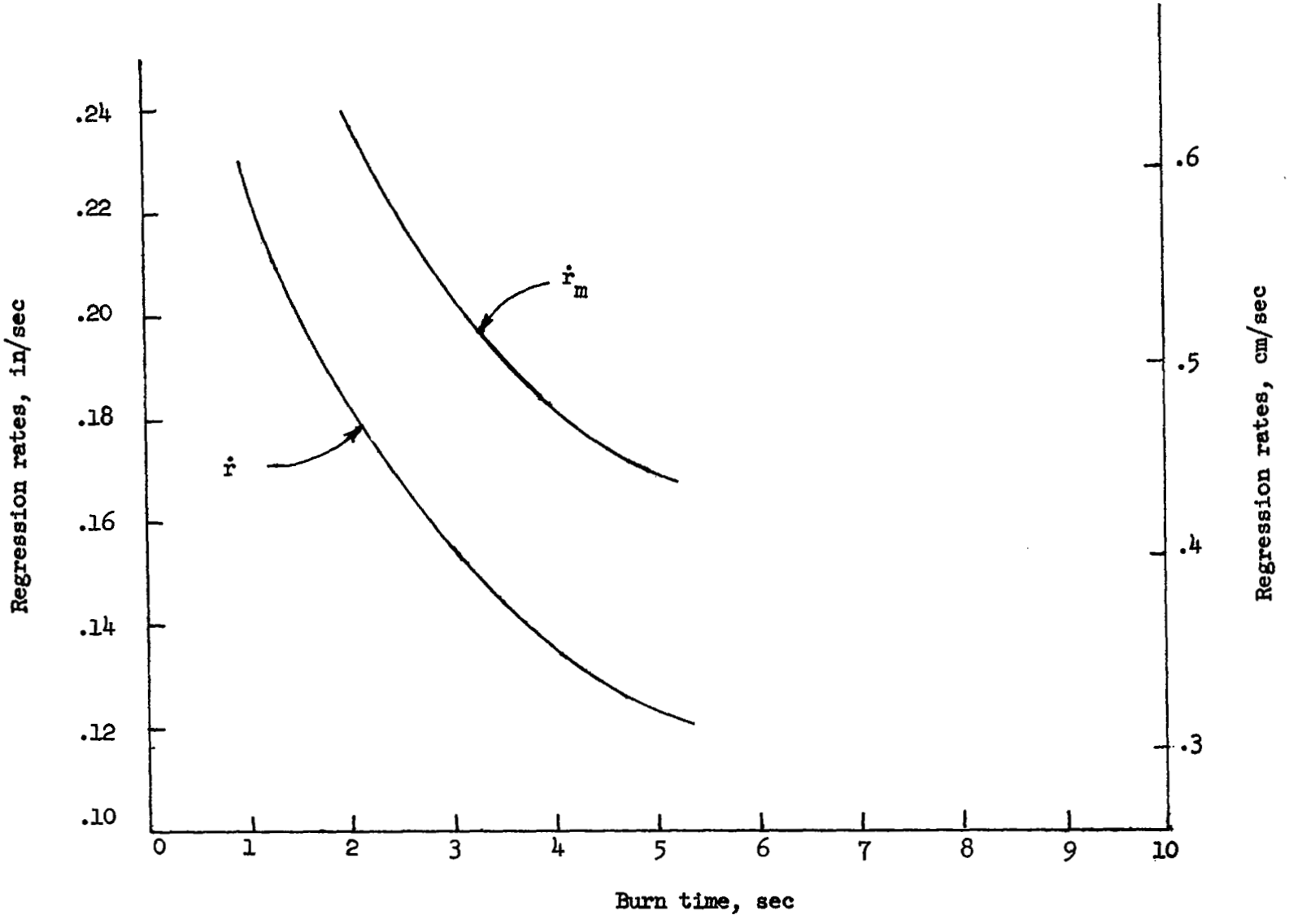

(d) 90-percent-lithium—10-percent-binder; $\dot{Q}$ = 45 Btu/in^2-sec $(73.53 \times 10^6$ W/m$^2)$ at time = 0; $\dot{Q}$ = 8.5 Btu/in^2-sec $(13.89 \times 10^6$ W/m$^2)$ at burnout.

Figure 7.- Concluded.

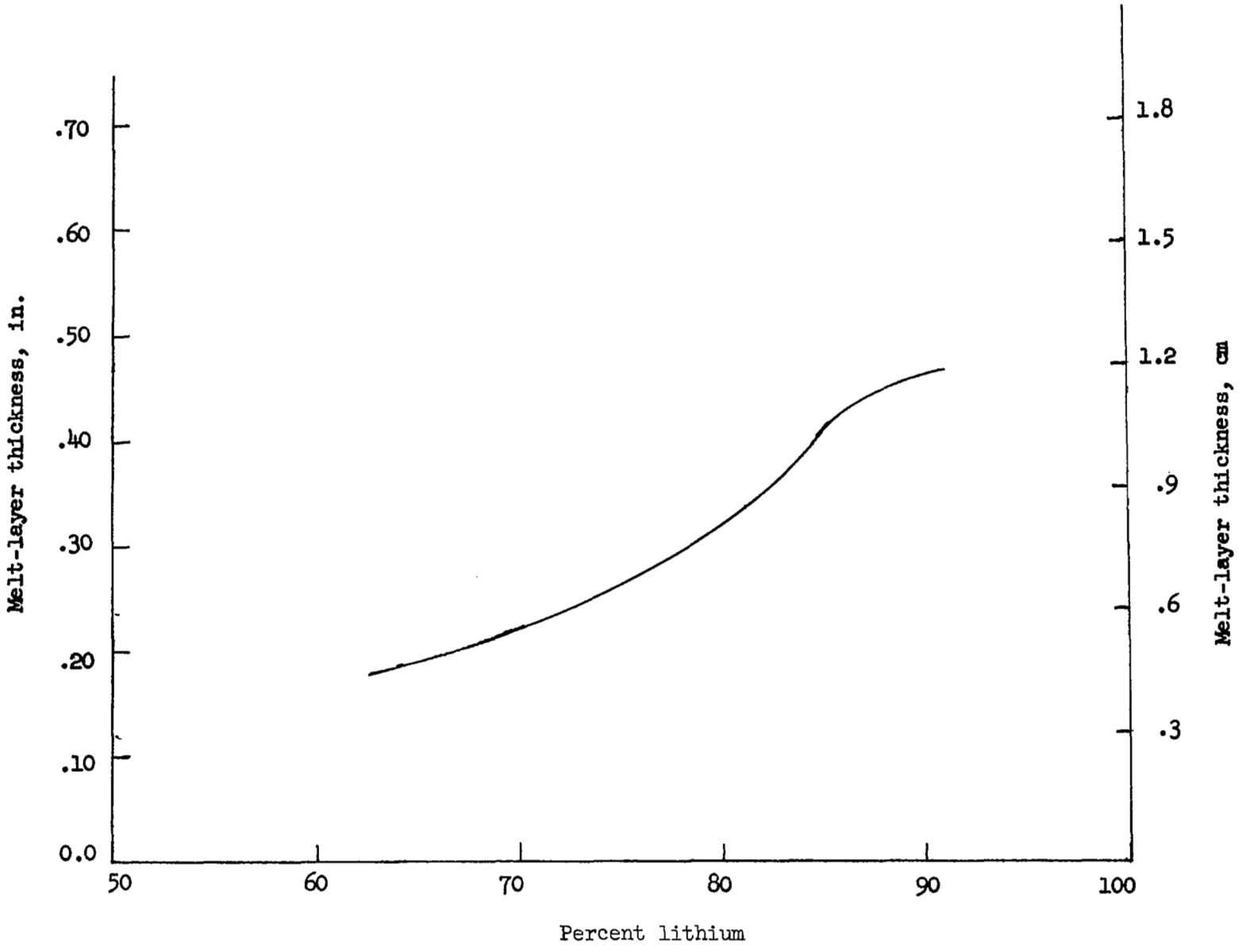

Figure 8.- Melt-layer thickness as function of percent lithium. Cylindrical grain values taken at burn time.

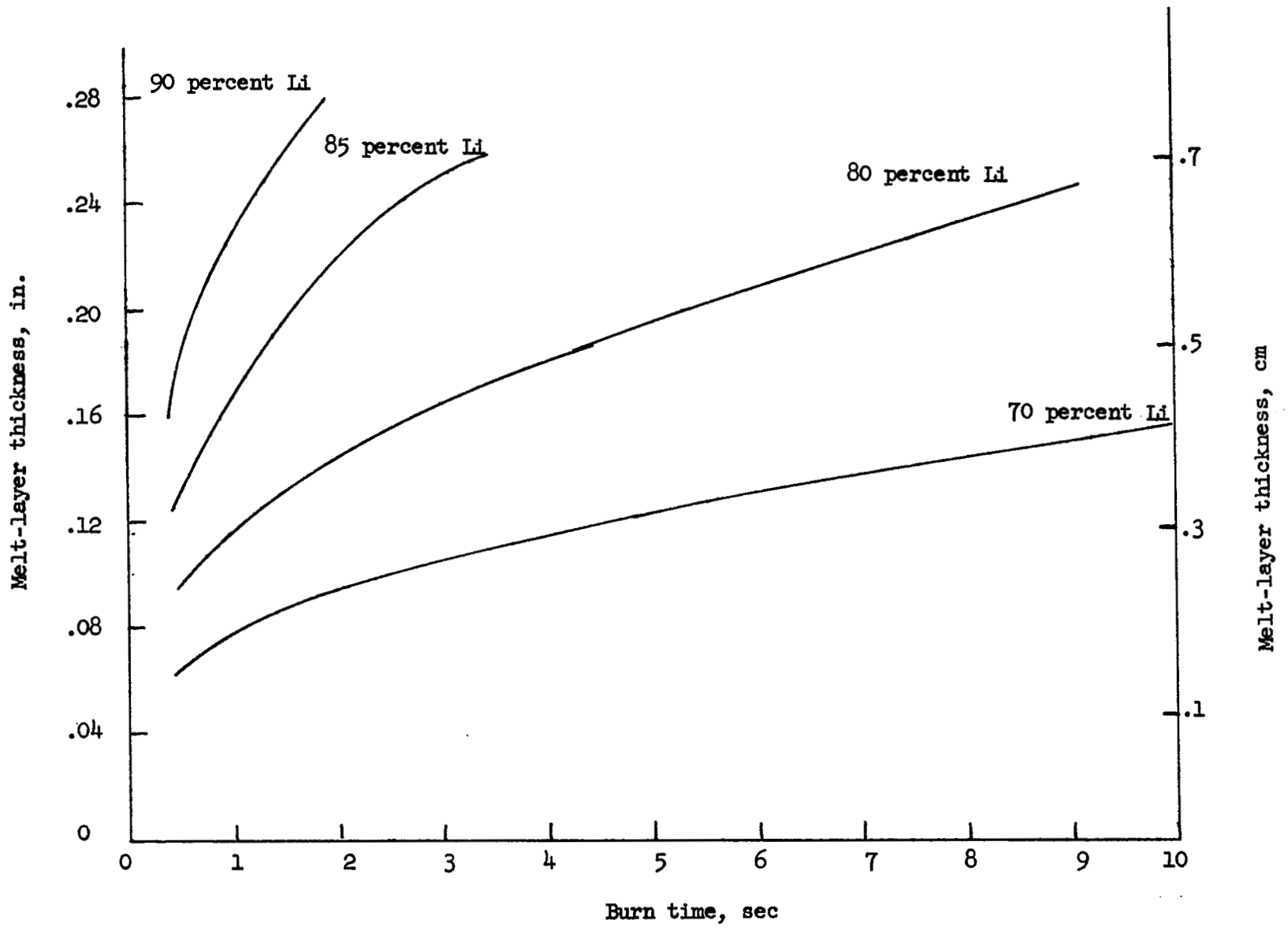

Figure 9.- Variation of melt-layer thickness with burn time. Cylindrical grain.

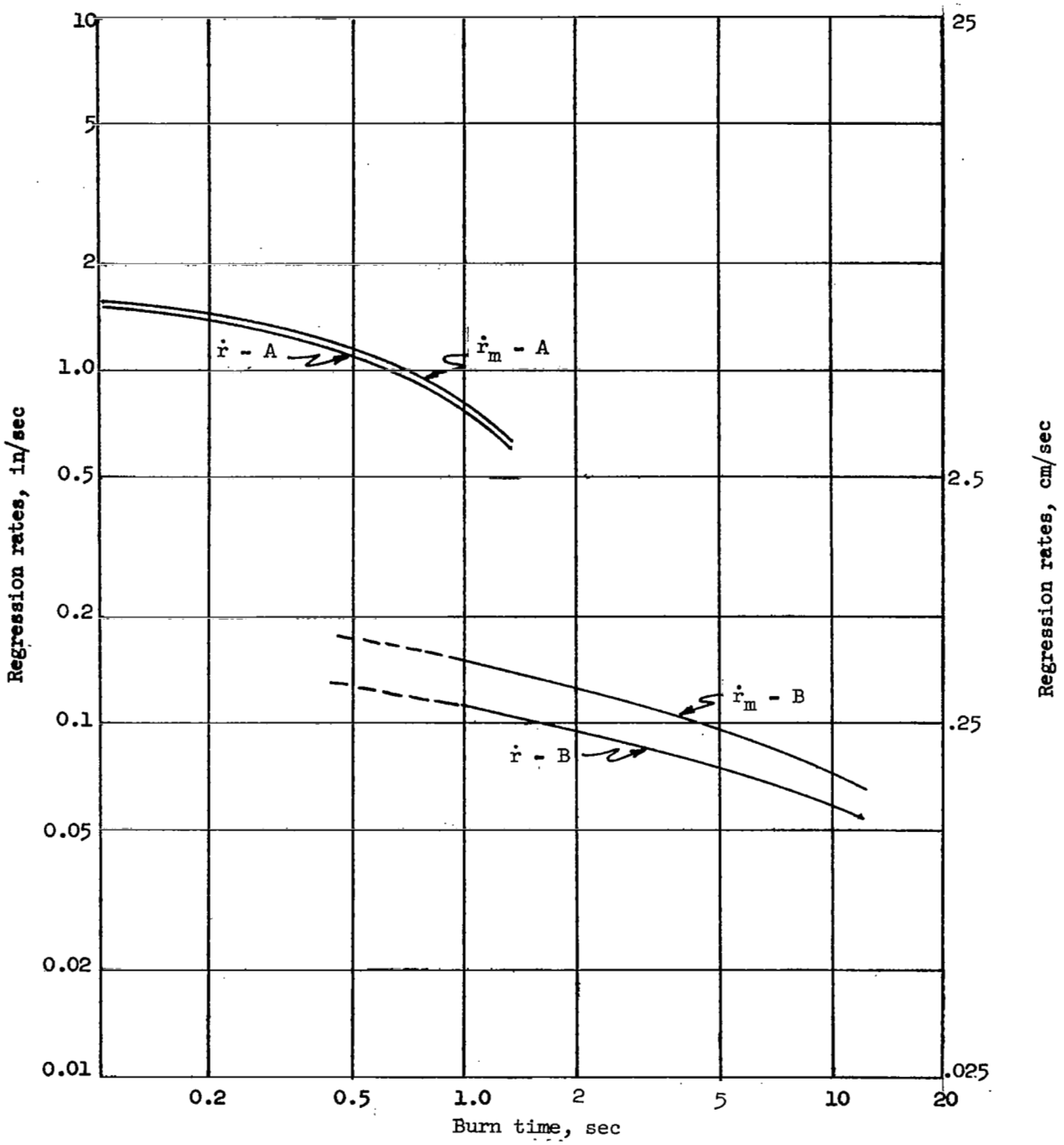

Figure 10.- Regression rates as function of burn time. Cylindrical grain, 80-percent lithium—20-percent-binder. Dashed lines indicate extrapolation.

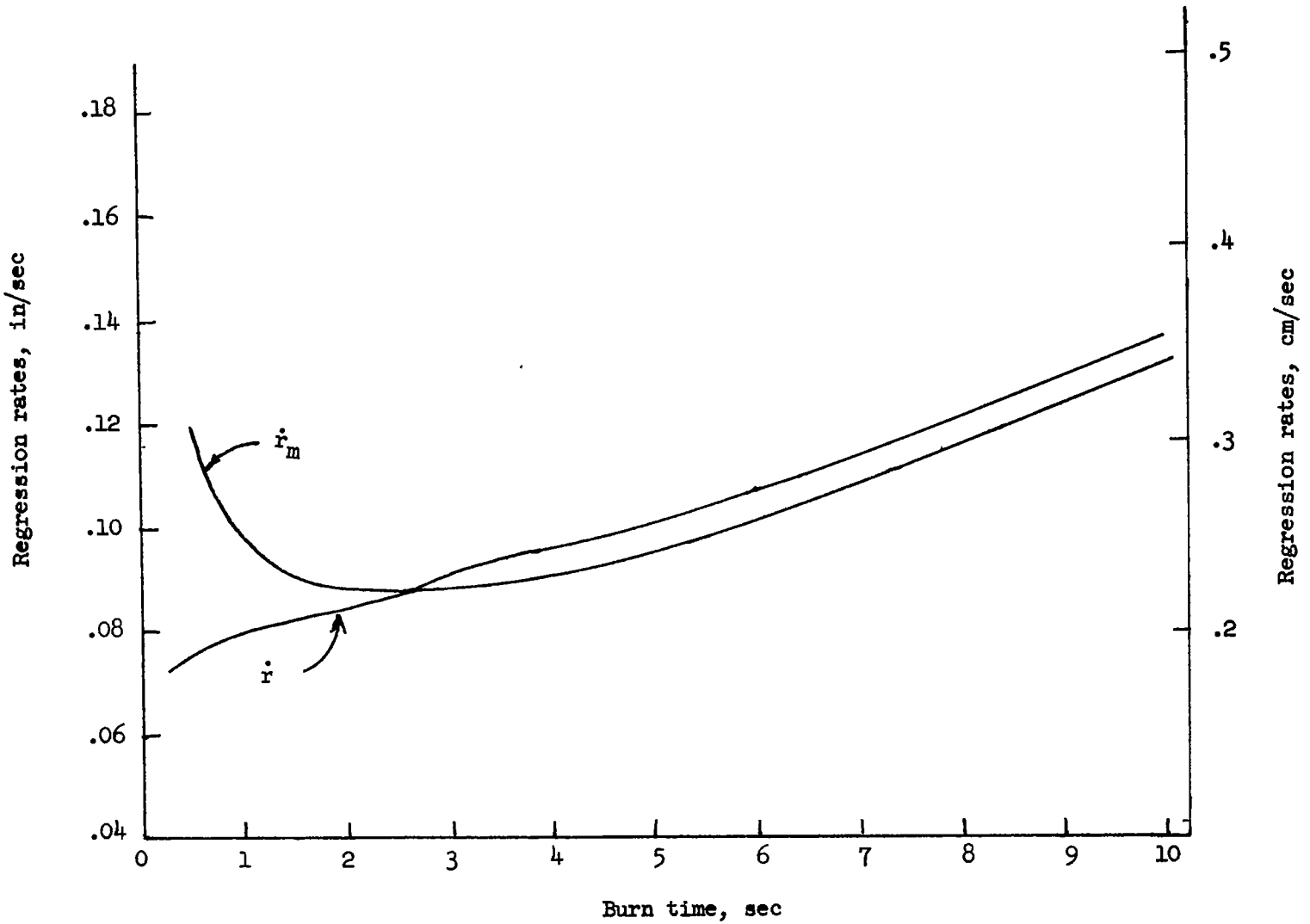

(a) 70-percent-lithium—30-percent-binder; heat input to surface increasing with time; $\dot{Q}$ = 6 Btu/in^2-sec $(9.8 \times 10^6$ W/m$^2)$ at time = 0; $\dot{Q} \doteq$ 12.7 Btu/in^2-sec $(20.75 \times 10^6$ W/m$^2)$ at burnout.

Figure 11.- Regression rates as functions of burn time. Hypothetical grain.

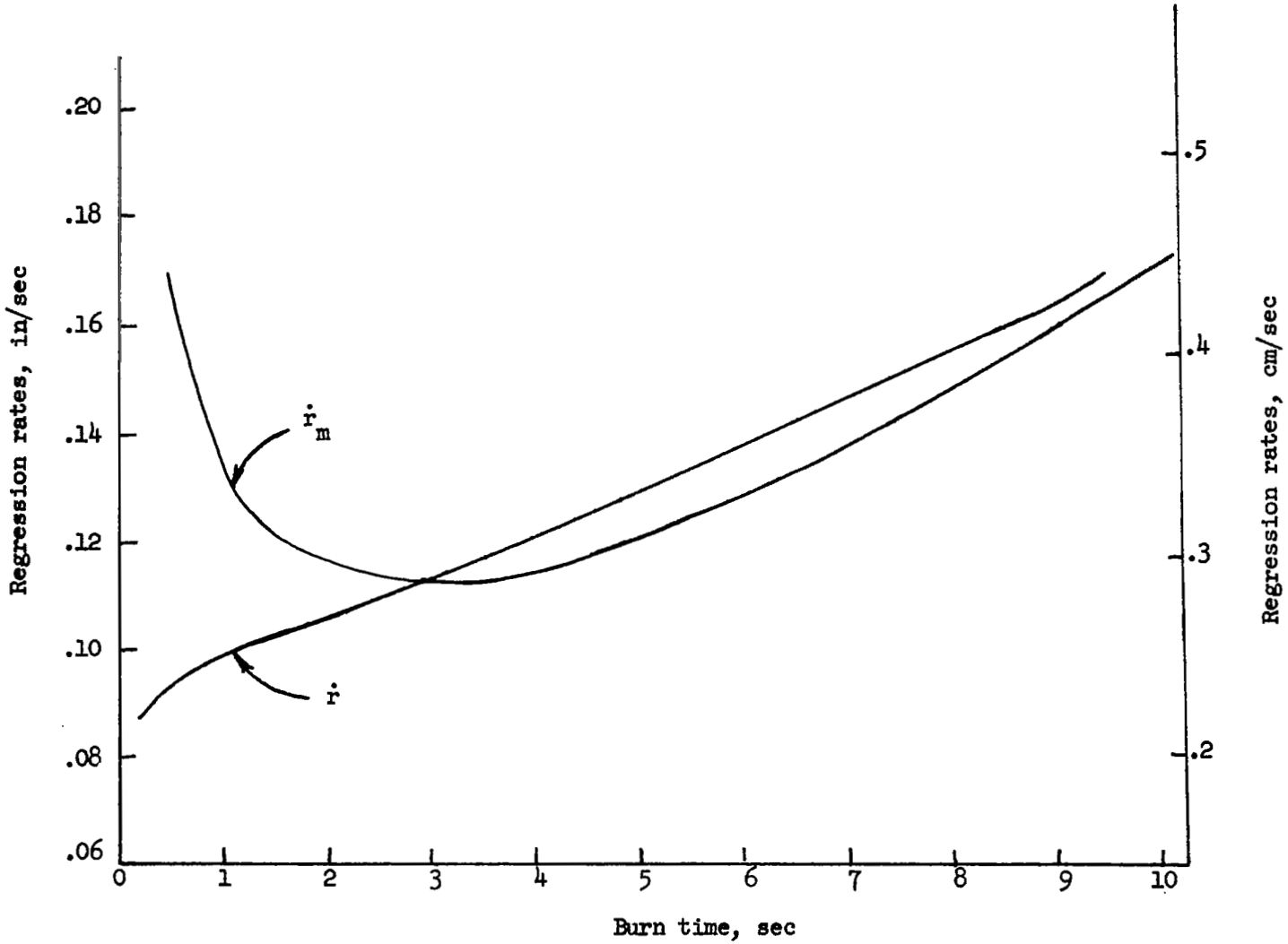

(b) 80-percent-lithium—20-percent-binder; $\dot{Q}$ = 10 Btu/in^2-sec $(16.34 \times 10^6$ W/m$^2)$ at time = 0; $\dot{Q}$ = 20 Btu/in^2-sec $(32.68 \times 10^6$ W/m$^2)$ at burnout.

Figure 11.- Continued.

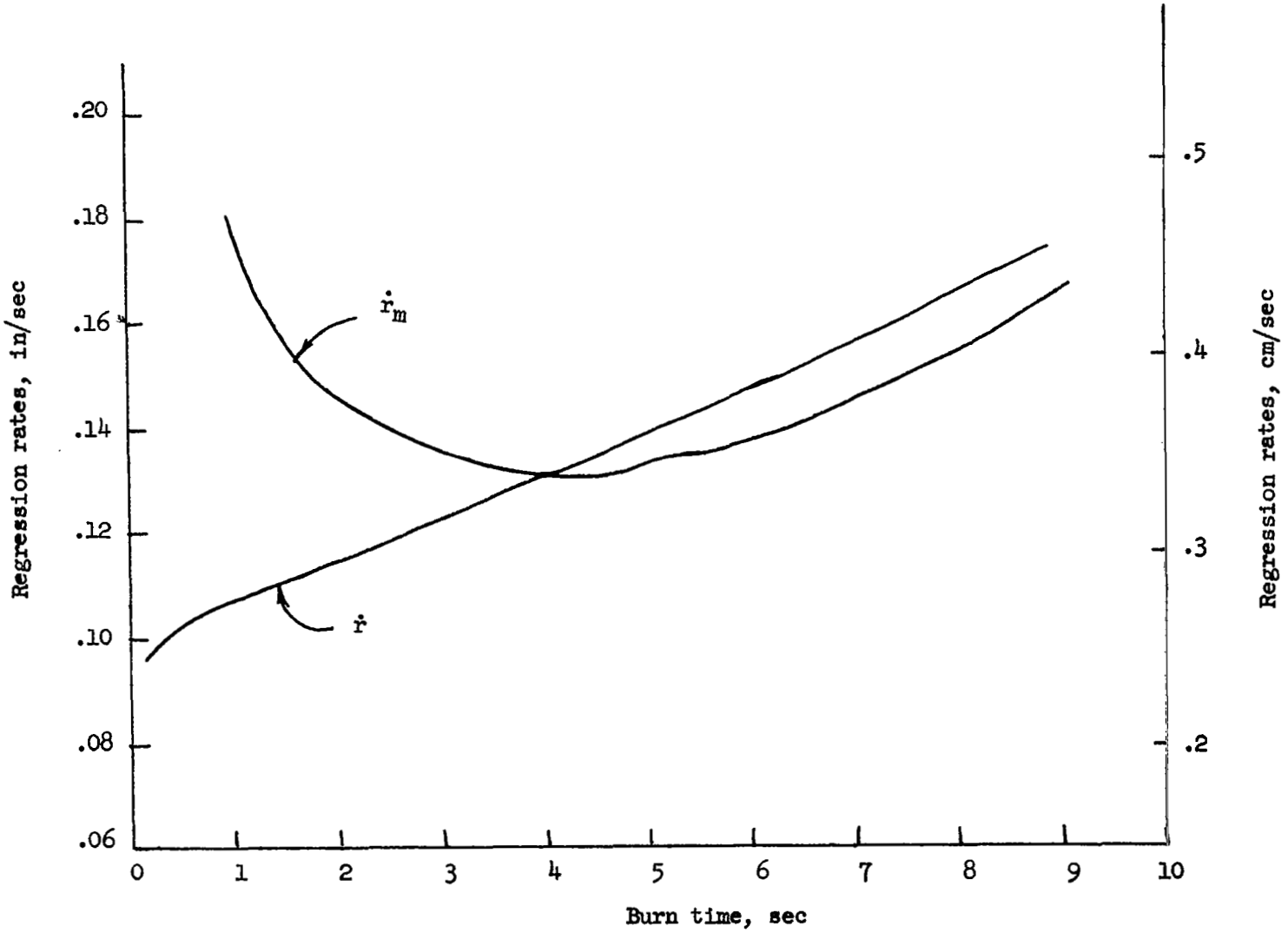

(c) 85-percent-lithium—15-percent-binder; $\dot{Q}$ = 15 Btu/in^2-sec $(24.51 \times 10^6$ W/m$^2)$ at time = 0; $\dot{Q}$ = 28 Btu/in^2-sec $(45.75 \times 10^6$ W/m$^2)$ at burnout.

Figure 11.- Continued.

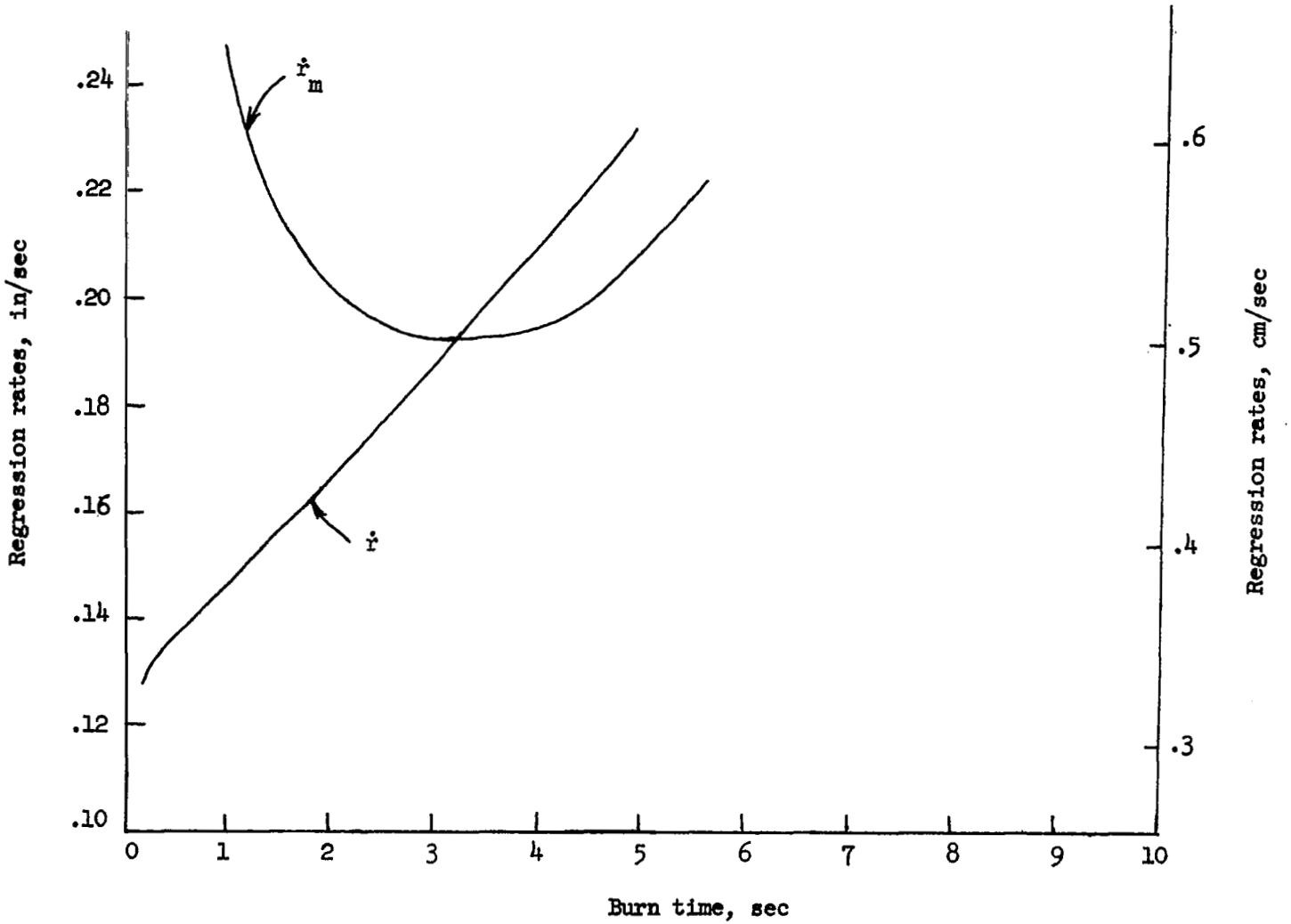

(d) 90-percent-lithium—10-percent-binder; $\dot{Q}$ = 20 Btu/in^2-sec $(32.68 \times 10^6$ W/m$^2)$ at time = 0; $\dot{Q}$ = 45 Btu/in^2-sec $(73.53 \times 10^6$ W/m$^2)$ at burnout.

Figure 11.- Concluded.

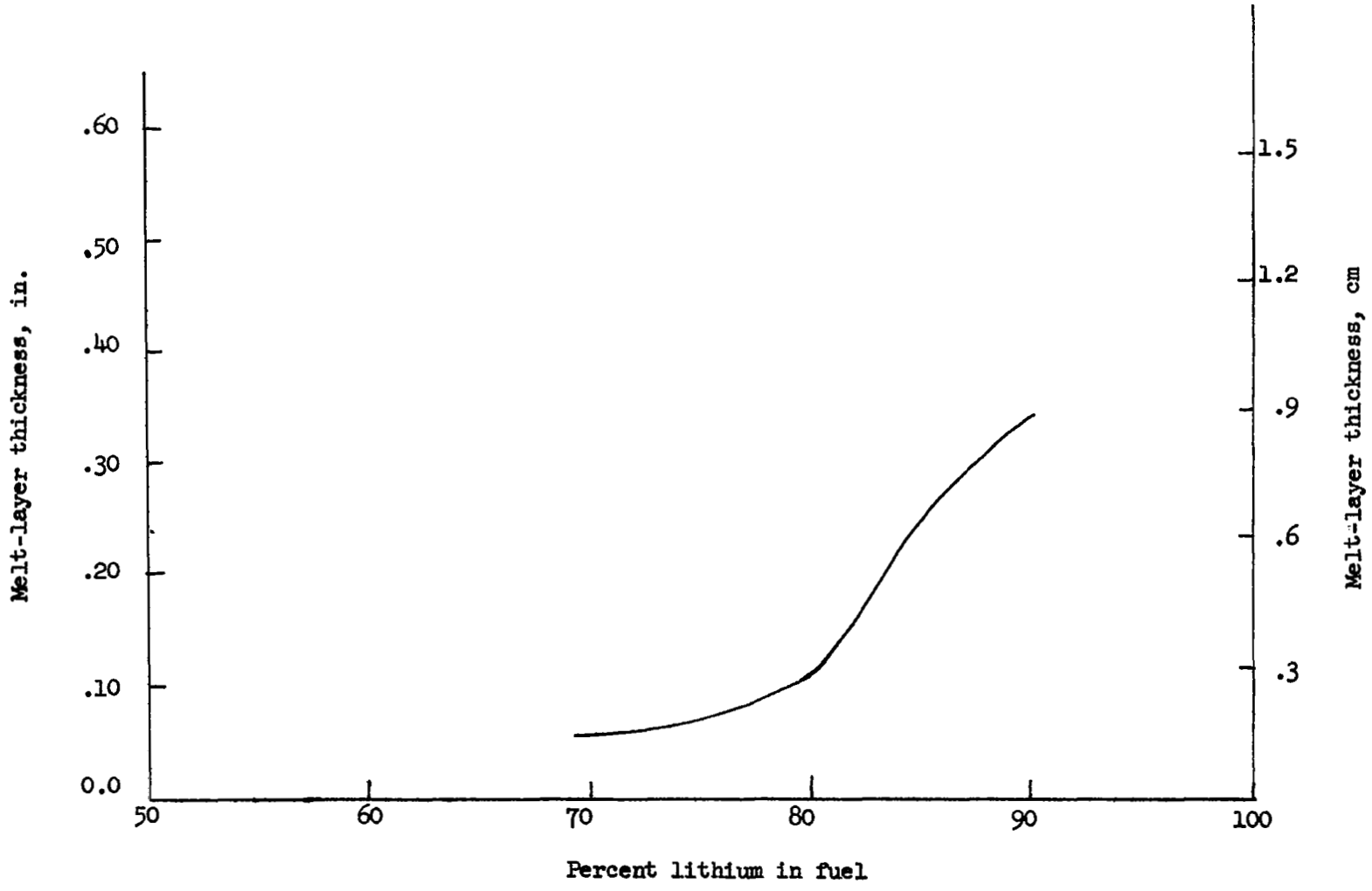

Figure 12.- Melt-layer thickness as function of percent lithium in fuel. Hypothetical grain; heat input to surface increases with time; melt-layer values taken at end of burn time.

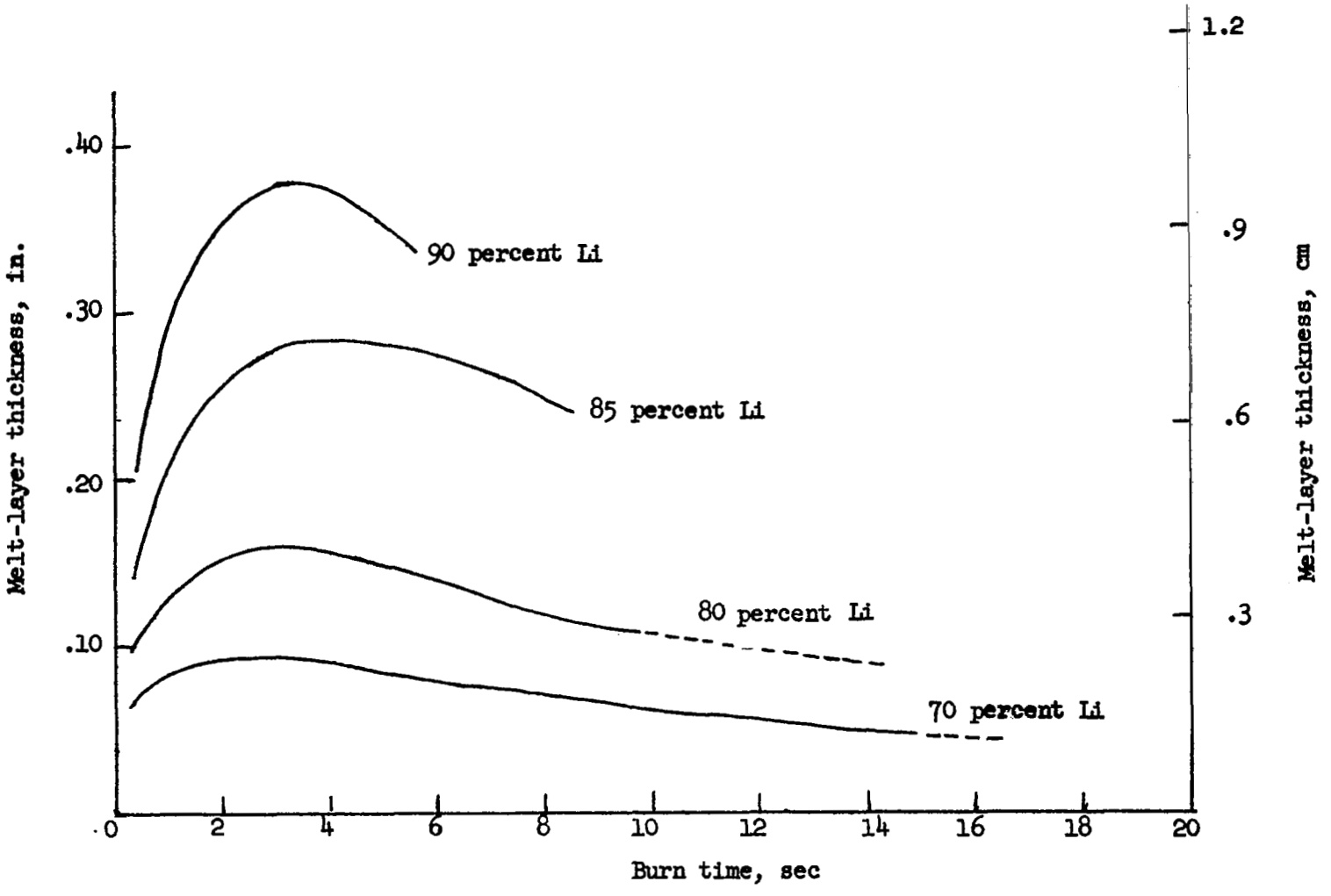

Figure 13.- Melt-layer thickness as function of burn time. Hypothetical grain; heat input to surface increasing with time.

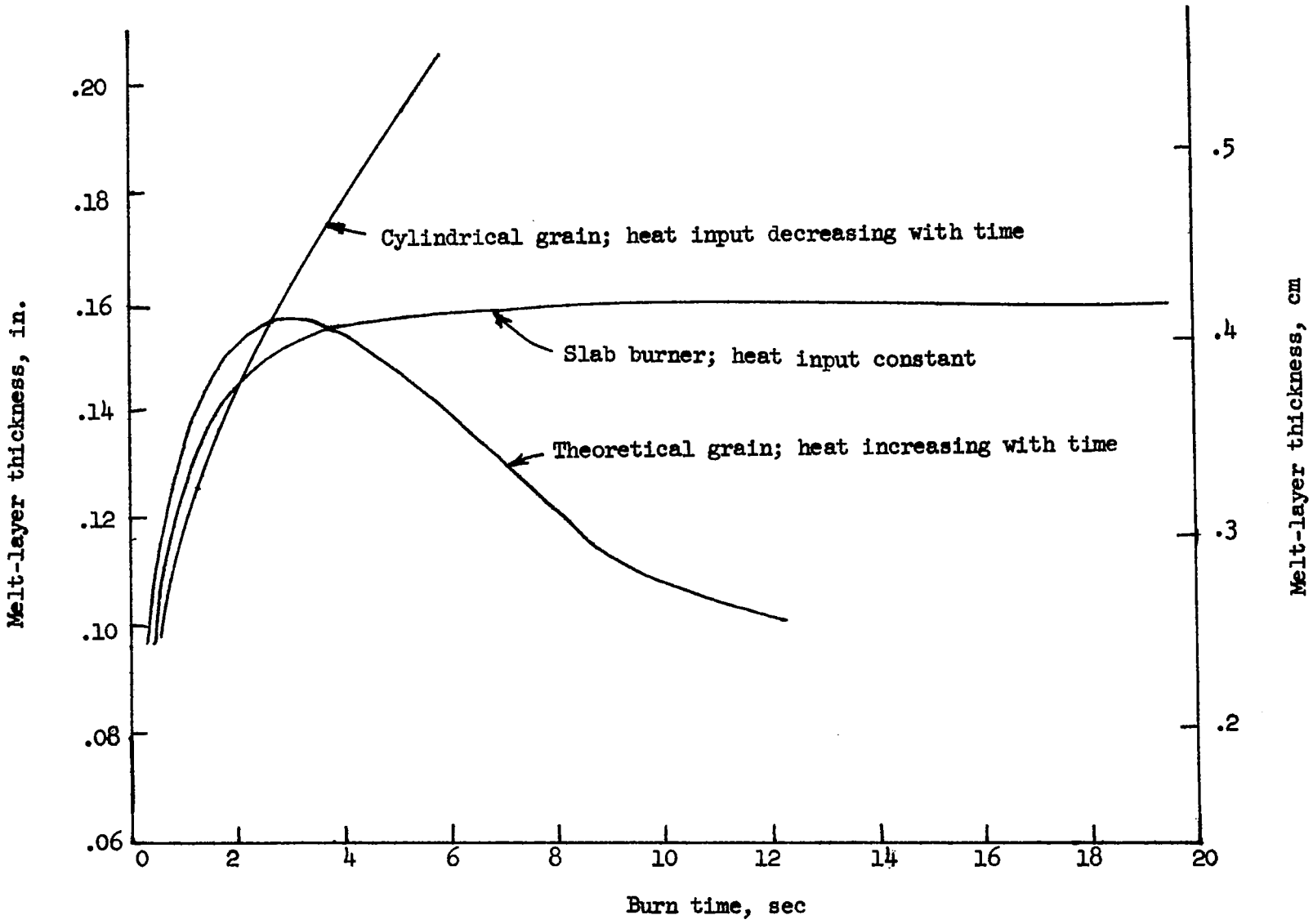

Figure 14.- Melt-layer thickness as function of burn time. All grain configurations of 80-percent-lithium—20-percent-binder.

NATIONAL AERONAUTICS AND SPACE ADMINISTRATION
WASHINGTON, D. C. 20546
OFFICIAL BUSINESS

FIRST CLASS MAIL

POSTAGE AND FEES PAI
NATIONAL AERONAUTICS
SPACE ADMINISTRATION

POSTMASTER: If Undeliverable (Section 1
Postal Manual) Do Not Re

"The aeronautical and space activities of the United States shall be conducted so as to contribute . . . . to the expansion of human knowledge of phenomena in the atmosphere and space. The Administration shall provide for the widest practicable and appropriate dissemination of information concerning its activities and the results thereof."

—NATIONAL AERONAUTICS AND SPACE ACT OF 1958

NASA SCIENTIFIC AND TECHNICAL PUBLICATIONS

TECHNICAL REPORTS: Scientific and technical information considered important, complete, and a lasting contribution to existing knowledge.

TECHNICAL NOTES: Information less broad in scope but nevertheless of importance as a contribution to existing knowledge.

TECHNICAL MEMORANDUMS: Information receiving limited distribution because of preliminary data, security classification, or other reasons.

CONTRACTOR REPORTS: Scientific and technical information generated under a NASA contract or grant and considered an important contribution to existing knowledge.

TECHNICAL TRANSLATIONS: Information published in a foreign language considered to merit NASA distribution in English.

SPECIAL PUBLICATIONS: Information derived from or of value to NASA activities. Publications include conference proceedings, monographs, data compilations, handbooks, sourcebooks, and special bibliographies.

TECHNOLOGY UTILIZATION PUBLICATIONS: Information on technology used by NASA that may be of particular interest in commercial and other non-aerospace applications. Publications include Tech Briefs, Technology Utilization Reports and Notes, and Technology Surveys.

Details on the availability of these publications may be obtained from:

SCIENTIFIC AND TECHNICAL INFORMATION DIVISION

NATIONAL AERONAUTICS AND SPACE ADMINISTRATION

Washington, D.C. 20546